Using Multi-mission Satellite Altimetry to Monitor Subglacial Hydrological Activities in the Totten Basin, East Antarctica

Jun Liu, Lihui Chen, Denghui Tang, Huan Xie, Xiangbin Cui, Peinan Li

***Abstract*—In East Antarctica, the largest thinning rates are observed at Totten Glacier in recent years. Hydrologic activity of the three active subglacial lakes (Totten$_1$, Totten$_2$, Wilkes$_1$) located on Totten Glacier may affect the ice sheet mass balance in the region on time scales of decades. In this study, we utilized laser altimetry data (ICESat and ICESat-2) and radar altimetry data (CryoSat-2 and Sentinel-3) to establish a 20-year time series of surface ice sheet elevation changes for three subglacial lakes, employing different least squares fitting methods, and this analysis aimed to study their hydrological activities. Additionally, we combined REMA and BedMachine data to acquire the subglacial drainage pathways in the region, analyzing the hydrological connections among the three subglacial lakes. The results indicate that Totten$_1$ and Totten$_2$ exhibited frequent inflow and outflow throughout the observation period, with periodic characteristics in lake activities. From 2003 to 2009, Wilkes$_1$ showed an ascending trend in surface ice sheet elevation, followed by a relatively stable state. The characteristics of lake activities changes and subglacial drainage pathways indicate connections among these three subglacial lakes. This study highlights that CryoSat-2 and Sentinel-3 radar data can fill the gaps between ICESat and ICESat-2 data. Furthermore, ICESat-2 laser altimetry data not only extend the records of subglacial lake activities but also capture more densely and accurately resolved spatial details. The integration of these four altimeters proves effective for long-term monitoring of active subglacial hydrological activities.**

***Index Terms*—Multi-mission data, satellite altimetry, subglacial lake activity, elevation change, Totten Glacier.**

I. INTRODUCTION

In recent years, the Antarctic ice sheet has been melting at an accelerated rate, contributing to a global rise in sea levels [1]. Totten Glacier is the fastest thinning region in East Antarctic and response for ice volume loss in the East Antarctic ice sheet, the changes in this region are essential indicators of global warming [2], [3]. The three active subglacial lakes (Totten$_1$, Totten$_2$ and Wilkes$_1$) are located beneath outlet glaciers in the Totten Glacier, the hydrological activity of them could affect ice sheet mass balance on time scales of decades [4]. In addition, because of the episodic nature of subglacial lake activity, with some lakes having cycles of about a decade or more, we need to monitor them continuously over time in order to fully understand them [5]. Therefore, continuous monitoring of the activities of the three active subglacial lakes in Totten Glacier using satellite altimetry technology is of significant importance. Subglacial lakes are bodies of water stored within cavities between the base of the ice sheet and the bedrock [6]. The hydrological activity of these lakes can be studied by monitoring changes in the surface elevation of the ice sheet over the lakes. Detection of subglacial lakes has become a focal point of interest for numerous researchers in recent years [7]. However, subglacial lakes have been regarded as independent and relatively stable bodies of water beneath the Antarctic ice sheet, forming isolated and enclosed systems for a long time [8], [9], [10]. It was not until 2005, with Gray's research, that it was demonstrated that in reality, subglacial lake water can flow, causing changes in the surface elevation of the ice sheet overlying the subglacial lakes [11], [12], [13]. Satellite altimetry technology has played a crucial role in the detection of subglacial lakes. Satellite altimetry has been greatly utilized in the detection of subglacial lakes, and with the development of satellite altimetry, the combination of different sources of altimetry satellites can provide long-term ice sheet elevation data with significant advantages such as wide coverage and high accuracy, which is not only utilized for identifying active subglacial lakes but has also become an essential means for monitoring their activities [14], [15], [16], [17].

Since the 1990s, a series of satellite radar altimetry technologies have been employed to measure changes in ice sheet elevation, including ERS-1 (RA), ERS-2 (RA), Envisat (RA-2), Sentinel-3 (SARL), and CryoSat-2 (SIRAL). These satellites utilize radar signals with relatively long wavelengths that can penetrate cloud cover, enabling continuous observations [18], [19], [20], [21]. Additionally, in recent years, laser satellite altimetry has been widely applied in polar regions. ICESat, operational from 2003 to 2009, and ICESat-2, launched in 2018, are two primary data sources for estimating ice sheet elevation. Compared to radar altimeters, laser altimeters have smaller footprints and higher measurement accuracy [22]. In conclusion, ICESat, CryoSat-2, and ICESat-2 data have become the main sources for studying the activities of subglacial lakes in Antarctica [23], [24], [25], [26]. However, due to limitations imposed by the effective lifespan of satellites and the inability of a single satellite to monitor the long-term evolution of ice

This work described in the paper was substantially supported by the National Natural Science Foundation of China (Project No. 42201489 and 42325106). *and the Shanghai Academic Research Leader Program [grant no. 23XD1404100] (Corresponding author: Huan Xie, Xiangbin Cui).*

Jun Liu, Lihui Chen, Denghui Tang are with College of Urban Railway Transportation, Shanghai University of Engineering Science, Shanghai 201620, China.

Huan Xie is with Shanghai Key Laboratory for Planetary Mapping and Remote Sensing for Deep Space Exploration, College of Surveying and Geo-Informatics, Tongji University, Shanghai 200092, China (huanxie@tongji.edu.cn).

Xiangbin Cui is with Polar Research Institute of China, Glaciology Division, Shanghai 200136, China (cuixiangbin@pric.org.cn).

Peinan Li is with College of Environmental Science and Engineering, Donghua University, Shanghai 201620, China.

sheet activities, combining measurements from multiple altimetry missions has proven to be an effective approach in establishing long-term ice sheet elevation change sequences.

As satellite altimeter data for extracting elevation changes continually updates, previous studies have integrated different altimetry missions to achieve more effective long-term elevation change monitoring. For instance, Siegfried et al. (2018) combined ICESat and CryoSat-2 data to sample 45 subglacial lakes in Antarctica, extending their elevation change time series until the end of 2016 [4]. Siegfried et al. (2021) utilized CryoSat-2 and ICESat-2 data to extend the activity time series of five lakes in CryoSat-2's SARIn mode until 2020 [27]. In addition, Zhang et al. (2020) combined radar altimetry data from Envisat and CryoSat-2 spanning from 2002 to 2019, and constructed an elevation change sequence for the Antarctic ice sheet using a planar fitting least squares regression model [7]. And Yang et al. (2022) combined datasets from three different altimeters (ICESat, CryoSat-2, and ICESat-2), utilizing a method involving cross-analysis and surface fitting to monitor the elevation change rates of the Greenland ice sheet from 2003 to 2020 [22]. Yi Fan et al. (2022) analyzed 17 active subglacial lakes in typical areas in Antarctica and extended the time series of the ice surface elevation changes combining CryoSat-2 and ICESat-2 data, the cross-validation of the two time series indicated a good agreement in flat surface of subglacial lake [28]. Furthermore, one of the critical issues in combining data acquired by various missions is bias correction. McMillan et al. (2013) corrected the bias between ICESat and CryoSat-2 by employing bilinear interpolation of the elevations of four surrounding CryoSat-2 measurement points at the location of each ICESat measurement point location outside $COOK_{E2}$ subglacial lake [29]. Differently, Zhang et al. (2020) and Li et al. (2022) incorporated parameters for the intermission and A-D (ascending and descending) biases between satellite altimeter missions into least-squares fitting model. They simultaneously corrected both types of biases to ensure the consistency of elevation time series between different missions[3], [7]. These two methods are bias-corrected before generating the time series, but can also be corrected after generating the single-mission time series. For example, Schröder et al. (2019), Paolo et al. (2016), Adusumilli et al. (2018), and Sørensen et al. (2018) applied bias correction at each cell by utilizing overlapping time from multiple-mission data [2], [30], [31], [32]. Lai et al. (2022) combined ICESat, CryoSat-2, and ICESat-2 data to establish a monthly elevation time series for the Greenland Ice Sheet from 2004 to 2020 [33]. The computation of inter-mission bias is estimated by fitting a linear model to the time series within a short time period. The deviation between the linear trends fitted for two different missions at the same location represents the inter-mission bias.

In previous studies on the Totten Glacier Basin in Antarctica, Qiuyang Zhao utilized ICESat laser altimetry data and a method of repeat-track least-squares plane fitting to calculate elevation and volume changes of the $Totten_1$, $Totten_2$, and $Wilkes_1$ subglacial lakes from 2003 to 2009 [34]. Subsequently, Siegfried et al. (2018) extended the elevation change time series of these three subglacial lakes to 2016 by incorporating CryoSat-2 data [4]. Then the following studies are all based on Totten Glacier, not the three subglacial lakes. Li et al. (2022), using CryoSat-2 and Sentinel-3 datasets, extracted elevation changes in the Antarctic ice sheet, revealing a negative growth trend in the Totten region from 2016 to 2019 [3]. Similarly, Zhang et al. (2020) combined Envisat and CryoSat-2 datasets to investigate elevation changes in the Totten region. Three locations were selected for the study, and the results indicated an overall negative trend in the average elevation changes from 2002 to 2019 [7]. Flament et al. (2012), employing Envisat radar altimetry data from 2002 to 2010, confirmed the dynamic thinning of the Totten Glacier [35]. Additionally, King et al. (2022) used new Global Positioning System (GPS) time series from the Totten-Denman Glacier region in East Antarctica to study the vertical movement of the ice sheet, indicating the highest average uplift rate of approximately 1.5 m/y in the Totten Glacier Basin from 2010 to 2020 [36].

In this study, we utilized data from four different satellite altimeters: ICESat (2003-2009), CryoSat-2 (2010-2023), Sentinel-3 (2016-2023), and ICESat-2 (2019-2023). Using the least squares fitting method, we monitored the surface elevation changes of $Totten_1$, $Totten_2$, and $Wilkes_1$ subglacial lakes in the Totten region. Finally, we integrated all the time series obtained from laser and radar altimetry to form a consistent and continuous elevation change time series covering nearly 20 years from 2003 to 2023. Moreover, CryoSat-2, Sentinel-3, and ICESat-2 have overlapping mission periods, allowing for mutual validation of the acquired time series.

II. Study Region and Data

A. Study Region

The Totten Glacier Basin is the largest glacier basin in East Antarctica, and the bottom melting of the ice sheet has led to the long-term negative mass balance of the Totten Glacier, playing a crucial role in the overall mass balance of Antarctica [37], [38]. The study area focuses on three subglacial lakes in the Totten region, namely $Totten_1$, $Totten_2$, and $Wilkes_1$ subglacial lakes. The lake outlines used in this study were obtained from ICESat data by Smith [39], with respective areas of 567 km^2, 710 km^2, and 569 km^2. $Totten_1$ is located downstream of $Totten_2$, while $Wilkes_1$ is situated at the furthest downstream position. As shown in Fig. 1, the upper left image represents the 100-meter resolution DEM (Digital Elevation Model) of Antarctica from REMA (Reference Elevation Model of Antarctica). The red box outlines the location of the Totten region in Antarctica. The main image provides information on the three subglacial lakes, and the colored background map represents the DEM of the region where these lakes are situated. The Totten region is located on the marginal area of Antarctica and falls within the coverage area of CryoSat-2 data in SARIn mode.

Based on previous studies, $Totten_1$ and $Totten_2$ had frequent inflow and outflow during 2003 to 2009. $Totten_1$ generally exhibited a pattern of drainage followed by refilling, while $Totten_2$ showed periodic variations, $Wilkes_1$ remained in a refilling state [34]. Additionally, during the period from 2010 to 2016, $Totten_1$ was generally in a refilling state, $Totten_2$ experienced slight

fluctuations, and $Wilkes_1$ remained stable [4].

B. ICESat Data

The ICESat satellite, the first satellite mission to carry a laser altimetry system for Earth observation, which operated from September 2003 to October 2009 at an orbit height of 600 km and an inclination angle of 94°, with a repeat cycle of 91 days that included a 33-day sub-cycle, the altitude accuracy of ICESat is about 15 cm [2]. Its coverage was extensive, capable of covering regions up to 86° of both North and South latitudes, and these data demonstrated a remarkable capability to assess changes in ice sheet elevation and sea ice thickness [40], [41], [42]. This study used the polar ice sheet elevation data ICESat/GLA12, the Geoscience Laser Altimeter System (GLAS) aboard the ICESat spacecraft is referenced to the Topex/Poseidon ellipsoid [43]. The data is Level-2 product and includes height information, laser footprint position information, equipment and atmospheric correction parameters, etc. Compared to other radar altimetry data, ICESat/GLA12 has a higher resolution and uses an algorithm specifically designed for the ice sheet surface to process the pulse waveforms. The laser pulse generates a footprint on the ground with a diameter of about 70 m and the space of approximately 17m along the track.

C. CryoSat-2 Data

CryoSat-2 was launched in April, 2010, with a 369-day fully repeating orbit and a 30-day subperiod. It is still in orbit at an altitude of 717 km and an inclination angle of 92°, and it can extend its coverage to a latitude of 88° [44], the altitude accuracy of the altimeter is about 50 cm for CryoSat-2 [2]. CryoSat-2 satellite is equipped with the Synthetic Aperture Interferometric Radar Altimeter (SIRAL), which operates in three modes: Low-Resolution Mode (LRM), Synthetic Aperture Radar (SAR) mode, and SAR Interferometric (SARIn) mode. The SARIn mode uses the phase difference between two onboard antennas to precisely determine the across-track location of the return echo within the SAR footprint [45]. The mode is active over areas of steep ice terrain, the ice sheet peripheries, ice caps, and mountain glaciers [46]. In SARIn, SIRAL uses two receiver antennae to perform interferometry, allowing the location of the point of closest approach (POCA) to be precisely determined in the across track plane, and Doppler processing is then used to reduce the along-track footprint to approximately 300 m [47]. SARIn mode is particularly well-suited for measuring steep and complex terrain at the edges of ice sheets. CryoSat-2 can reach centimeter-level observation accuracy in challenging terrain compared with previously launched radar satellites [48]. In this study, we used Baseline-D Level2 SARIn mode data ranging from 2010 to 2023. The product uses the TFMRA (Threshold First Maximum Retracker Algorithm) retrack algorithm to process the waveforms on top of the Baseline-C L1b product, and adds interferometric processing for phase and coherence, allowing the Baseline-D product to provide better elevation measurements. improving the ascent and descent cross-statistics from 1.9 to 0.1 m, substantially reducing the impact of track deviation on the estimation of ice surface elevation changes [44], [49].

D. Sentinel-3 Data

Sentinel-3 was initially designed for ocean observation, with its main objectives being to measure sea surface topography, monitor ocean and land surface temperatures, provide support for marine forecasting systems, and monitor environmental and climate changes [50]. Sentinel-3 mission consists of four satellites. Sentinel-3A (S3A) was launched in February 2016, Sentinel-3B (S3B) followed with its launch in April 2018, and the planned launches for Sentinel-3C/D are scheduled to take place after 2021 [51]. S3B's orbit is positioned so the ground separation between S3A to S3B tracks is half that of the individual ground separation of each satellite. The Sentinel-3 satellite has an observation range of up to 81.35°S, with a repeat observation period of 27 days, and utilizes a Ku-band SAR altimeter. In comparison to CryoSat-2, Sentinel-3 is less well equipped to monitor changes to ice sheets and the 27-day repeat cycle means it has a significantly larger ground separation. However, on the interior of the ice sheet, where CryoSat-2 uses LRM mode, Sentinel-3 is the first satellite radar altimeter to deploy SAR altimetry. In these regions, Sentinel-3's delay-doppler processing decreases the footprint size in the along-track direction to ~300 m compared to the larger LRM footprint [52]. Consequently, high resolution elevation measurements are acquired for the first time in the ice sheet interior, the precision and accuracy over the low sloping interior to be on the order of 10 cm but both decreased over more complex topography [53]. Moreover, compared to CryoSat-2, the 27-day repeat cycle of Sentinel-3 provides higher temporal resolution, allowing for repeated track elevation measurements at nearly monthly time intervals and potentially enabling the direct observation of seasonal changes over the ice sheets. Considering the existing issues with CryoSat-2 exceeding its operational limits, Sentinel-3 altimetry data can offer new data assurances for monitoring the elevation of the Antarctic ice sheet. This is of significant value in studying the long-term temporal changes in ice sheet elevation.

E. ICESat-2 Data

The ICESat-2 satellite was launched in September 2018, which serves as a successor to ICESat, which continues to provide elevation information on polar sea ice and ice cover. It carries a single micro-pulsed photon-counting laser that covers a range of up to 88 ° S with a 91-day repeat cycle [54]. ICESat-2 laser is split into six individual beams in three pairs. The beams in a pair have different transmit energies (energy ratio of ~1:4) and are separated by 90 m in the across-track direction. This configuration means that ICESat-2 has a finer spatial sampling resolution compared to ICESat and CryoSat-2, the altitude accuracy of ICESat-2 is about 10 cm [2]. Compared with the laser on ICESat that sends 40 pulses per second, the ICESat-2 laser is fast-firing and sends 10,000 pulses per second, so ICESat-2 has denser footprints than ICESat. The multibeam instrument design, smaller footprint, and the ability to resolve rougher terrains enable more accurate elevation measurements and fewer measurement gaps [55]. The ICESat-2 data product used in this paper is ATL06, which belongs to the Level 3A land ice elevation data product. The spatial resolution of the ATL06 data product is 20 m, the accuracy of the height inversion is better than 0.03 m and the accuracy for determining the rate of change of surface elevation change on ice sheets is approximately 0.4 cm/y. Table S1 summarizes the altimetry data used in the study.

F. REMA and BedMachine Data

REMA (Reference Elevation Model of Antarctica) is a high-resolution digital elevation model released by the Polar Geospatial Center (PGC) in the United States. It covers the Antarctic land ice region from 60°S to 88°S [56]. The version utilized in this study is at a 100 m resolution. Based on 47 airborne ice penetrating radar data from 1967 to 2020, which was used by Morlighem et al. to generate ice thickness data (BedMachine) covering the entire Antarctic through mass conservation, streamline diffusion, and other methods [57]. BedMachine set contains a bed topography map of Antarctica deduced by subtracting the ice thickness from the surface elevation taken from the Reference Elevation Model of Antarctica (REMA) [57]. This paper used bed topography of BedMachine version V3 with a resolution of 500 m. These datasets are employed in this study for calculating hydraulic potential, obtaining the drainage pathways of subglacial lakes, and subsequently analyzing the hydrological connections among the three subglacial lakes.

III. Methodology

Fig. 2 shows the entire flowchart of the methodology for monitoring the hydrological activities of three subglacial lakes in the Totten Glacier Basin by integrating multi-mission altimetry data. The proposed approach consists of three main components, as follows: (I) preprocessing operations for different types of altimetry data; (II) bias exists between different missions, and different bias correction methods as well as different least-squares fitting models are selected to establish the time series of elevation changes according to different data types; and (III) simulating the drainage pathways of subglacial lakes based on ice surface elevation data and subglacial bedrock data. Further details of the proposed approach are provided in the following sections.

A. Data preprocessing

The observation process of ICESat laser altimetry system is subject to many factors that can lead to a large number of errors in the resulting observations. Therefore, filtering and error correction preprocessing operations are required, including correction of the ICESat mission bias and observation error correction. During laser radar distance measurement, the selection of the reference pulse can cause errors in the acquired surface elevation, reaching up to ±6 cm in Antarctica [58]. When calculating the surface elevation annual change rate, this leads to an increase in the elevation change trend by 0.92 to 1.90 cm/y [59]. In this study, each point of ICESat was geographically corrected using the G-C (centroid vs. Gaussian, G-C) correction program released by NSIDC. Additionally, for observational errors caused by instruments, atmosphere, and surface reflection, data filtering and corrections were performed according to the criteria in the literature [60]. Then the corrected ICESat altimetry data was converted to heights above the WGS84 ellipsoid to ensure consistency with the coordinate systems of ICESat-2 and CryoSat-2.

The CryoSat-2 Level2 data we used incorporated a series of geophysical corrections, including slope correction, dry atmospheric correction, wet atmospheric correction, tropospheric correction, ionospheric correction, solid Earth tides correction, and ocean tides correction [61]. Additionally, for ice shelves, extra corrections such as inverse barometric correction and ocean tide correction were applied. We further applied a 3σ filter and removed echoes with abnormally high backscatter (bs>30 dB) to eliminate anomalous data [4], [28].

For the other radar data (Sentinel-3), we utilized Level-2 Sentinel-3A data from March 2016 to June 2023 and Level-2 Sentinel-3B data from June 2018 to June 2023. The secondary processing of SAR mode data primarily provides preliminary retracked elevation estimates for oceans, coastal zones, ice sheets, and sea ice. Moreover, the precision and accuracy of the S3A and S3B satellite SAR models are comparable in the Antarctic region, and these two satellites can be used interchangeably to study the ice sheet evolution [62]. The Level-2 data have been slope-corrected. Subsequently, similar to the approach applied to CryoSat-2 data, this study conducted data filtering based on the 3σ criterion and backscatter coefficient.

For ICESat-2 data, in order to utilize the most reliable ICESat-2 ATL06 data subsets for fitting the reference surface, it is necessary to filter and screen the downloaded initial data. The specific steps are as follows:

1) Firstly, filter out data points with ATL06_quality_summary = 0 based on the quality label provided in the ATL06 data. ATL06_quality_summary is calculated based on residual spread, along-track surface slope, estimated errors, and signal strength for each segment. It can be initially used to remove unqualified data.

2) ATL06 contains some segments with signal-finding blunders. To avoid having these erroneous segments contaminate the final accuracy of the results, we determined the parameter AT_min_dh based on surface roughness. We identified high-quality ATL06 segments, using parameter AT_min_dh. The parameter AT_min_dh is defined as the minimum absolute difference between the height at each endpoint of a data segment and the height at the center point of the preceding and succeeding segments. For smooth surfaces, a value less than 2 meters is required. However, if the remaining data is less than one-third of the original cycle after removing data based on the smooth surface criterion, then it is considered a rough surface. In this case, the requirement is relaxed to value of the parameter less than 10 meters [63]. According to these criteria, we further keep the higher-quality ATL06 data based on the topographic surface roughness.

3) A high degree of overlap in the orbits is required for the repeated orbit method. However, through the analysis of ATL06 data products, it is observed that in some cycles, there is a significant deviation from the original orbit. This phenomenon is attributed to a configuration error in the tracker during the early stages of the ICESat-2 mission, preventing the instrument from accurately pointing to the reference orbit. As a result, there is a 1 to 2-kilometer offset between the observed trajectories in the first and second cycles and the reference orbit. Calculating elevation changes using the repeat orbit method under such conditions introduces significant errors. Therefore, it is necessary to exclude data with severe orbit deviations and retain data with better repeatability for further calculation.

4) For smooth or rough surfaces, an additional check is performed on each data segment using the parameter h_li_sigma. If the h_li_sigma value of points in the segment is greater than the maximum value between 0.05 and three times the median of h_li_sigma, the data point is removed. This additional step aims to further enhance the quality of the data used in the calculation [63].

B. Create time series of elevation changes

1) Least-squares plane fitting based on ICESat repeat tracks

According to the design requirements of the ICESat altimetry satellite orbit and its operational cycle, trajectory overlap occurs after a certain period, and all arcs along the same ground track are referred to as repeat tracks, and the time required to form repeat tracks is termed the repeat cycle. In this study, we filtered all ICESat data passing through the three subglacial lakes from 2003 to 2009 based on repeat tracks. Initially, repeat tracks were preliminarily determined based on orbit numbers. However, even with the same orbit number, there were cases of excessive separation between tracks, indicating non-repeat tracks. Therefore, a precise determination of repeat tracks was performed based on the distance between trajectories. Subsequently, the ICESat repeat track elevation data for each group were divided into rectangular cells with a length of 700 meters along the track direction and a width of 350 meters in the across-tack direction, with a 200-meter overlap between adjacent cells to ensure computational continuity. Finally, a least squares fit was applied to the elevation data within each rectangular cell to obtain the rate of elevation change and terrain features for each cell. For accurate fitting, at least 2 repeat tracks passing through each subglacial lake, each with a minimum of 6 repeat arcs and a minimum of 10 points within each rectangular cell, were ensured during the least squares fitting. The mathematical model used for least squares regression included estimating east-west slope, north-south slope, elevation change rate (dh/dt or vertical movement speed), and residuals (res), and the following mathematical model was used:

$$H = a_0 + a_1 x + a_2 y + a_3 t + res \tag{1}$$

where a_0 is the elevation at the cell center; a_1 is the slope in the x-direction; a_2 is the slope in the y-direction; a_3 is the rate of elevation change; and *res* represents the residuals.

Let $Y = \begin{bmatrix} H_1 \\ \vdots \\ H_n \end{bmatrix}$ $B = \begin{bmatrix} 1 & x_1 & y_1 & t_1 \\ \vdots & \vdots & \vdots & \vdots \\ 1 & x_n & y_n & t_n \end{bmatrix}$ $\hat{X} = \begin{bmatrix} a_0 \\ a_1 \\ a_2 \\ a_3 \end{bmatrix}$ then the error equation for the above model (1) is formulated as:

$$V = Y - B\hat{X} \tag{2}$$

The least squares estimate is:

$$\hat{X} = (B^T PB)^{-1} B^T PB \tag{3}$$

In Eq. (2), *V* is the column matrix of correction values for the observed values, and in Eq. (3), *P* is the weight matrix of the height differences, which is assumed to be 1 in this paper. After obtaining the estimated values of the parameters, the accuracy of the parameters is obtained according to the following formula:

$$Q_{XX} = (B^T PB)^{-1} \tag{4}$$

$$\sigma_0 = \sqrt{V^T PV/(n-t)} \tag{5}$$

where Q_{XX} is the covariance matrix of the three parameter estimates; σ_0 is the unit weight standard deviation; n is the number of observed points in the cell; t is the number of unknown parameters, and here $t = 4$. Consequently, the slope, elevation change rate, and errors for each cell can be calculated based on these equations.

2) Least squares surface fitting on a regular cell using CryoSat-2 and Sentinel-3 data

Firstly, this study divided the CryoSat-2 and Sentinel-3 radar altimetry data within each subglacial lake region into a cell of 3 km × 3 km based on the location of each subglacial lake, and calculated the coordinates of the center point for each cell. Because the elevation results monitored by different missions may have deviations and the ascending and descending orbit data of the radar altimeter tend to be offset due to the effect of orbital anisotropy, the intermission bias and A-D bias between the same missions need to be taken into account when solving using the least squares model. In this paper, the descending orbit data of CryoSat-2 is used as the baseline, and the deviations of the ascending orbit data of CryoSat-2, the ascending orbit data of Sentinel-3, and the descending orbit data of Sentinel-3 from the baseline data are set as the parameters CS_aCS_d, SEN_aCS_d, and SEN_dCS_d to be added to the fitting model. Finally, the least squares model (Eq. (6)) was used to fit the altimetry data within each cell, obtaining the rate of elevation change. Moreover, the 3σ anomaly removal criterion is applied, followed by iterations. After each iteration, data points with an absolute value of the average elevation change greater than 10 meters are removed as outliers until no more data points are excluded. Then the elevation change rate is obtained after outlier-removed data is exported. The model for the least squares repeat-track algorithm is as follows:

$$H = a_0 + a_1 x + a_2 y + a_3 x^2 + a_4 y^2 + a_5 xy + a_6 t + a_7 bs + CS + res \tag{6}$$

where $a_0 - a_7$ are the model parameters corresponding to the variables mentioned above; *bs* represents the backscatter coefficient; *CS* is the bias between CryoSat-2 and Sentinel-3(see Eq. (7)); *res* represents the residuals.

$$CS = CS_aCS_d(-1)^{CS_aCS_d} + SEN_aCS_d(-1)^{SEN_aCS_d} + SEN_dCS_d(-1)^{SEN_dCS_d} \tag{7}$$

According to the least squares estimation model, using the footpoint data as observed values, an error equation is constructed. Based on the least squares algorithm, the 11 parameters in this model are estimated.

3) Dynamic least squares fitting model based on ICESat-2 repeat tracks

The ATL06 product consists of 3 pairs of 6 beams each, with a separation of 90 meters between beams within each pair and 3.3 kilometers between pairs, and this paper took each pair of data as a processing unit for the repeat track calculation. Compared with the other three kinds of data, ICESat-2 ATL06 data has a large volume and dense distribution. To fully utilize the data, rectangular cells are defined along the track, with specific criteria: 100 meters along the repeat track direction, 200 meters across repeat track direction, and a 50-meter overlap between adjacent cells along the track. The next step involves the inversion of the reference surface shape, solving for the reference

surface and a set of corrected-height values, that represent the time-varying surface height at the reference points. The inversion process of this dynamic model mainly involves three matrices:

(a) The polynomial surface shape matrix *S*, which describes the spatial part of the inversion as a basis function.

$$S = \left[\left(\frac{x - x_{center}}{l_0}\right)^p \left(\frac{y - y_{center}}{l_0}\right)^q\right] \quad (8)$$

here x and y are the coordinates of the data points; x_{center} and y_{center} are the coordinates of the center point of cell; l_0 is the scaling factor that ensures the components of S are on the order of 1, thus improving numerical precision. We set $l_0 = 100$m, which is approximately match the intra-pair beam spacing. The most important aspect of this matrix is the calculation of the polynomial degrees p and q. The rules for calculation are: p and q cannot be 0 at the same time, the number of choices is not more than 3 (in the along-track direction) or 2 (in the across-track direction), thus p is not more than 3, q is not more than 2, and the sum of p plus q in the same term must not be more than 3. Additionally, p should not exceed the number of different y values in the pair (in the across- track direction), and q should be less than the number of different x values by at least 1(in the along- track direction) in any cycle, with the distinct values in each direction defined at a resolution of 20 m.

(b) The matrix *D* represents the height-change component of the inversion.

For the same rectangular cell, there are various cycles of data points, each cycle of the observed elevation of $h_1, h_2 \ldots h_{19}$, then the height of the data points in the cell can be represented as:

$$D \times H = \begin{bmatrix} 1 & 0 & 0 & \cdots & 0 \\ 0 & 1 & 0 & \cdots & 0 \\ 1 & 0 & 0 & \ldots & 0 \\ 0 & 0 & 0 & \cdots & 1 \\ \vdots & \vdots & \vdots & \vdots & \vdots \\ 0 & 0 & 0 & \cdots & 1 \end{bmatrix}_{n\times 19} \begin{bmatrix} h_1 \\ h_2 \\ h_3 \\ h_4 \\ \vdots \\ h_{19} \end{bmatrix}_{19\times 1} \quad (9)$$

here: n is the number of data points in the rectangular cell, and D matrix is a 0-1 matrix preceding the elevation matrix.

(c) The slope change matrix S_t describes the linear rate of change in the surface slope in the along-track and cross-track directions during the mission period.

$$S_t = \left[\left(\frac{x - x_0}{l_0}\right)\left(\frac{t - t_0}{\tau}\right), \left(\frac{y - y_0}{l_0}\right)\left(\frac{t - t_0}{\tau}\right)\right] \quad (10)$$

where: t represents the observation time of the data points, t_0 is equal to the midpoint between the start of the repeat track pointing and the end of the mission. The time scale factor τ is equal to one year (86400 * 365.25 seconds).

Estimating the surface shape, slope changes, and height time series is achieved by forming a composite design matrix *G*:

$$G = [S\ S_t\ D] \quad (11)$$

The least squares estimate is:

$$\hat{X} = (G^T G)^{-1} G^T H \quad (12)$$

To calculate the errors in subsequent results, this study constructed the covariance matrix C_m:

$$C_m = ((G^{-g} G)^{-1} G^T) C_1 ((G^{-g} G)^{-1} G^T)^T \quad (13)$$

In Eq. (13), we constructed a diagonal matrix C_1, with the diagonal values being the maximum of $h\_li\_sigma^2$ and $RDE(res)^2$, where RDE is the robust difference estimator. Schematic representation of the three fitting models is shown as Fig.S1 in appendix.

4) Correction of biases between multi-mission time series

We handled the mission biases in two main parts, for two satellite data (CryoSat-2 and Sentinel-3) with the same measurement principle (radar), we set their deviations to three parameters, which are added to the least-squares fitting model to solve (see Eq. (6)).

For the three types of data (ICESat, the fusion results of CryoSat-2 and Sentinel-3, and ICESat-2), which have different measurement principles (laser and radar), we corrected the mission bias in terms of time series. For ICESat, which has no overlapping time period with the radar data, we selected stable areas throughout the time period to estimate a linear change by fitting the time series of the two missions in the neighboring time, and then calibrated time series based on the difference between the linear changes. For ICESat-2, which has overlapping periods with radar data, we selected data from the overlapping periods for correction, following the same procedure as for ICESat. The following are the steps:

Firstly, based on different data and using various least squares models, single-mission time series are formed (see Fig. 3(a)), and then regions with a constant rate of change throughout the time period (cells with a change rate less than 1 cm/y) were selected to estimate a linear variation by fitting the time series of two missions at adjacent times, and calibrated based on the difference between the linear variations (see Fig. 3(b)). The data period for the fitting is from 2006 to 2014 for aligning ICESat and CryoSat-2 with Sentinel-3, and from 2020 to 2023 for aligning CryoSat-2 with Sentinel-3 and ICESat-2. After correcting the bias between the different missions, the time series of the three individual tasks were combined to form a consistent and continuous sequence of long-term elevation changes (see Fig. 3(c)).

C. Basic Principles of Subglacial Drainage Path Detection

Subglacial lake locations and volumes are determined by subglacial hydrology, and the flow and storage of subglacial water are controlled by the basic hydraulic potential. Liquid water beneath the ice sheet flows outward under the influence of subglacial water pressure potential, impacting the underlying bedrock topography and converging into subglacial drainage pathways. Therefore, the analysis of water pressure potential can be employed to deduce drainage pathways. Shreve proposed that water pressure potential is a function related to the ice surface elevation and bedrock elevation [64]. The calculation formula is:

$$\emptyset = \rho_i g Z_s + (\rho_w g - \rho_i g) Z_b \quad (14)$$

where $\emptyset$ is the hydraulic potential in units of pressure; ρ_i(971 kg/m^3) and ρ_w(1000 kg/m^3) are the densities of ice and water, respectively. Z_s and Z_b represent the heights of the ice surface and bedrock relative to the geodetic datum, and g is the gravitational acceleration.

Dividing both sides of Eq. (14) by the unit weight of freshwater ($\rho_w g$) transforms it into water pressure potential in units of elevation:

$$\emptyset' = \frac{\emptyset}{\rho_w g} = \frac{\rho_i g Z_s + (\rho_w g - \rho_i g) Z_b}{\rho_w g} = \frac{\rho_i}{\rho_w} Z_s - \frac{\rho_w - \rho_i}{\rho_w} Z_b \quad (15)$$

This study utilized ice surface elevation data from the REMA dataset and bedrock elevation data from the BedMachine dataset to calculate hydraulic potential. The depression filling model from the hydrological analysis module in the ArcGIS toolkit was employed to fill local depressions, resulting in a depression-free raster map of hydraulic potential. Subsequently, models for flow direction, flow accumulation, and river network classification were applied to obtain the final drainage pathways.

IV. Results

A. The elevation change results for Totten$_1$

This study first calculated the elevation change rates for all ICESat repeat tracks in the study area. The analysis revealed consistent elevation change rates in the subglacial lake region, allowing the determination of the basic locations of three subglacial lakes and the repeat track numbers of ICESat elevation data passing through each subglacial lake. The tracks covering Totten$_1$ are Track 107 and Track 145, and it can be seen from the rate of change graph (Fig. 4) that the average elevation change of Totten$_1$ is decreasing during the period of 2003 to 2009, the average rate of change of the elevation in the lake is -0.122 ± 0.06 m/y.

Fig. S2 depicts the error ($\sigma_{dh/dt}$) in the average change rate of Totten$_1$ subglacial lake from 2003 to 2009. Points with larger errors are distributed in areas with rough terrain (rough surface), and overall, the errors within the lake are larger than those outside the lake. This is attributed to the more frequent activity within the lake compared to the surrounding areas.

After determining the repeat tracks passing through subglacial lake and the average elevation change rates for each track, the elevation change rates for each repeat track were multiplied by relative time to calculate the elevation change, and the elevation change was interpolated to obtain the length of the repeat track in the lake. Fig. 5 shows the elevation change results for Track 107 and Track 145 passing through Totten$_1$ subglacial lake, representing the elevation change during different periods of ICESat missions. The positions of the two red vertical lines indicate the intersection points of the repeat track with the lake boundary, where L1 and L2 represent the lengths of the repeat tracks within the lake. The interpolated lengths are approximately 28 km for L1 and 42.5 km for L2. From these two figures, it can be observed that Track 107 and Track 145, these two repeat tracks, exhibit consistent elevation change trends over time. From September 2003 to June 2005, the surface elevation of the Totten$_1$ ice sheet was continuously decreasing, reaching a maximum decrease of about 5 meters in November 2005. Subsequently, an increase in water volume led to a rising trend in surface elevation, with a slow increase of about 1 meter from November 2005 to November 2006. From November 2006 to November 2008, a rapid increase in water volume caused the surface elevation of the ice sheet to rise by about 3 meters.

For the elevation change monitoring from 2010 to 2023, this study combined the use of CryoSat-2 and Sentinel-3 data. As shown in Fig. S3, the trend of surface elevation change for the Totten$_1$ subglacial lake is not constant during the period from 2010 to 2023. As shown in Fig. 6, from 2010 to 2019, the average elevation change exhibits a slow increasing trend, with an average rate of 0.09 ± 0.01 m/y. Moreover, from 2019 to 2023, the elevation change accelerates, showing a faster increase with an average rate of 0.2 ± 0.06 m/y. Overall, there is a pattern of gradual increase followed by a more rapid ascent, and the activity within the lake is significantly more pronounced than outside the lake.

To validate the precision of the elevation change results obtained from CryoSat-2 and Sentinel-3 altimetry data, this study incorporated ICESat-2 satellite altimeter data to monitor the elevation changes of the three subglacial lakes from 2019 to 2023. There are 11 repetitive tracks passing through the subglacial lake of Totten$_1$, Fig. 7 represents the average change rate from 2019 to 2023 calculated from ICESat-2 data, the maximum value of 0.98 ± 0.03 m/y is obtained at (-69.99°S, 107.38°E). The cell containing the location of the peak value (red box in Fig. 6(b)) includes this point, and the peak value is 0.979 ± 0.12 m/y consistent with the monitoring results of ICESat-2. Although the measurement principles of the two types of data are different and we used different fitting methods for the two types of data, the final elevation change results are spatially distributed consistently and numerically almost identical. And the two red vertical lines in Fig. 8 represent the intersection points of repeated tracks with the subglacial lake boundary, displaying the elevation change results for Track 1139 (the first beam pair) and Track 1192 (the first beam pair). The elevation change trends of the two tracks are generally consistent within the Totten$_1$ subglacial lake, exhibiting an increase followed by a decrease. The elevation change shows a continuous increase from March 2019, reaching a maximum elevation increase of approximately 4 meters around October 2022, followed by a slight decrease.

B. The elevation change results for Totten$_2$

As shown in Fig.9, the tracks covering Totten$_2$ are Track 11, Track 211, and Track 130, and the mean elevation change of Totten$_2$ is decreasing from 2003 to 2009, and the mean rate of elevation change in the lake is -0.19 ± 0.05 m/y. Fig.S4 represents error of the average elevation change rate.

Fig.10 shows the results of elevation changes of Track211 and Track130 covering the subglacial lake of Totten$_2$ (Track11 is not shown). The length L1 of Track 211 in the lake is about 36 km, and the length L2 of Track 130 in the lake is about 29.5 km. Furthermore, it can be seen that Totten$_2$ is more active than Totten$_1$ in this time period. From October 2003 to June 2005, the surface elevation of the Totten$_2$ ice sheet consistently decreased, reaching a maximum decline of about 2 meters in June 2005. Additionally, the elevation change trends of the three tracks are not consistent over time, the reason is that when the water flows to different areas of the subglacial lake, the subglacial terrain and blockage lead to deviations in the time of elevation change in each area [5].

As shown in Fig. S5, it can be observed that the overall mean elevation change of Totten$_2$ subglacial lake during the period of 2010-2019 had small fluctuation. As shown in Fig. 11, the average elevation change showed a slow rising trend with a rate of 0.07 ± 0.02 m/y from 2010 to 2019; in the period from 2019 to 2023, there was a faster rising trend with an average elevation

change rate of 0.2 ± 0.005 m/y. The overall trend of slow rise and then rapid rise is basically consistent with the trend of Totten$_1$ subglacial lake in this time period.

The ICESat-2 ATL06 data passed through the Totten$_2$ subglacial lake with a total of 22 repetitive tracks, Fig. 12 represents the average change rate from 2019 to 2023 calculated from ICESat-2 data, the maximum value of 0.79 ± 0.02 m/y is obtained at (-70.75°S, 110.9°E). The cell containing the location of the peak value (red box in Fig. 11(b)) includes this point, and the peak value is 0.79 ± 0.13 m/y consistent with the monitoring results of ICESat-2. And the positions of the two red vertical lines in Fig. 13 indicate the intersections of the repetitive tracks with the boundary of the subglacial lake. The elevation change results for Track 887, involving two pairs beam, exhibit a consistent trend. And the elevation changes in the range of the subglacial lake of Totten$_2$ are first increasing and then decreasing, firstly increasing continuously from March 2019 and reaching a maximum increase of about 2.4 m in October 2021, and then decreasing, with a maximum decrease of 0.5 m.

C. The elevation change results for Wilkes$_1$

The tracks covering Wilkes$_1$ include Track 145 and Track 130. As shown in Fig. 14, it is evident that Wilkes$_1$ experienced an average elevation increase from 2003 to 2009, with an average rate of change of elevation of 0.22 ± 0.03 m/y. Fig.S6 represents error of the average elevation change rate.

Fig. 15 shows the results of elevation changes of Track 145 and Track 360 covering the Wilkes$_1$ subglacial lake, the length of L1 in the lake is about 31 km and L2 is about 28 km. The elevation trends of Track 145 and Track 360 are consistent, showing a continuous ascent in the surface elevation of the Wilkes$_1$ ice sheet from 2003 to 2009. Before 2006, there was a slow increase, with an increase of 0.8 ± 0.04 meters in November 2006. After November 2006, the water level accelerated, resulting in the maximum elevation of the ice surface in November 2008, reaching an increase of 3 ± 0.09 meters.

The Wilkes$_1$ subglacial lake remained in a steady state during 2010-2023(see Fig. S7 and S8), without significant drainage or filling, and with less overall activity. ICESat-2 data encompass a total of 16 repeated tracks over Wilkes$_1$ subglacial lake. The elevation changes along these repeated tracks do not exhibit pronounced variations, as not explicitly presented in the paper. This lack of discernible elevation changes indicates a relatively stable condition with minimal water filling or drainage activities during this period, suggesting that the lake's water, once filled during the ICESat period, remained stored, maintaining a stable state from 2010 to 2023.

D. Establishing a continuous time series of mean elevation changes

Considering the topographic differences beneath the ice leading to temporal deviations in elevation trends among various repeated tracks and cells, this study employed a weighted average to generate a mean elevation change sequence within the subglacial lake. Additionally, accounting for the influence of snow accumulation and other driving force events, in this paper, we defined a rectangular outside the lake of size two times the length and width of the lake as a buffer area. We consider that mean elevation change within the buffer area outside the lake outline represents long-term changes of ice sheet. The relative average elevation change sequence within the lake was calculated by subtracting the average elevation change within a buffer area outside the lake outline from the average elevation change inside the lake (see Fig. 16). The average surface elevation of the Totten$_1$ subglacial lake experienced a decrease of approximately 2 meters from October 2003 to November 2005, followed by an ascent of 1.5 meters from November 2005 to March 2009. During the period from 2003 to 2009, there was a sequence of drainage followed by water influx activities. From 2011 to 2019, the lake remained relatively stable, and from 2019 to 2023, there was a water influx leading to an elevation increase of about 2 meters. The Totten$_2$ subglacial lake exhibited frequent inflow and outflow activities from 2003 to 2009, demonstrating periodic variations. The maximum descent during this period was approximately 1 meter. From 2011 to 2019, it remained relatively stable with a slight upward trend. Subsequently, the average elevation continued to increase, with a maximum rise of about 1.5 meters. The average surface elevation of the Wilkes$_1$ subglacial lake consistently increased from 2003 to 2009, with a maximum rise of around 1 meter. Subsequently, there were no significant drainage or water influx activities, maintaining a stable state until 2023.

To validate the accuracy of the time series in this study, we compared our results with previously published research (See table 1 for details). Qiuyang Zhao utilized ICESat data and employed the least squares method to calculate the elevation changes of three subglacial lakes from 2003 to 2009 [34], and the trend and the size of the peaks in this paper were in high agreement with them. Siegfried not only utilized ICESat data but also integrated CryoSat-2 data, extending the elevation time series of these three subglacial lakes to 2016 using the differential DEM method [4]. Our research results for this time period exhibit good consistency with theirs, with some slight discrepancies that may be attributed to differences in the calculation methods employed. In summary, the outcomes of this study demonstrate a certain level of reliability, respectively.

E. Hydrologic paths between subglacial lakes

After analyzing the dynamic characteristics of the three subglacial lakes, this study utilized REMA and BedMachine data to generate a drainage path map for the Totten Glacier basin. As shown in Fig. 17, the base map represents hydraulic potential, blue lines depict the paths of water flow, and black lines indicate the positions and outlines of the three subglacial lakes. The water potential energy in the region gradually decreases from around 2500 m in the northwest direction to approximately 1500 m in the southeast direction. Combining the topography and drainage paths, it can be inferred that the main flow direction of subglacial water in this region is from northwest to southeast, ultimately flowing towards the Budd Glacier. Totten$_1$ subglacial lake is located downstream of Totten$_2$ subglacial lake, and Wilkes$_1$ subglacial lake is situated at the furthest downstream position. Moreover, Totten$_1$ and Wilkes$_1$ are located in the different sub-tributaries of same main stream, and Totten$_2$ is located in the tributary of the other main stream.

V. Discussion

A. Bias between the CryoSat-2 and Sentinel-3 missions

In this study, two different radar data with overlapping observation times were added to the same fitting model to fuse the mission bias between different missions with the AD bias between the same missions and correct for both parts of the bias in a single calculation. Fig. 18 demonstrates the results of the three bias parameters of CryoSat-2 and Sentinel-3 in Eq. 9, Fig. 18(a) represents the parameter CS_aCS_d, Fig. 18(b) represents the parameter SEN_aCS_d, and Fig. 18(c) represents the parameter SEN_dCS_d. It is evident that even within the same mission, discrepancies exist between ascending and descending tracks. The deviation between the ascending and descending tracks of CryoSat-2 is mostly within 1 meter, with higher discrepancies, up to 4 meters, observed in topographically complex regions, as indicated by terrain analysis. From Fig. 18(b)(c), it can be seen that the bias between CryoSat-2 descending orbit data and Sentinel-3 ascending and descending orbits is quite large, which is due to the fact that the Sentinel-3 data has a large footprint compared with the CryoSat-2 SARIn data and the accuracy is not as good as that in the interior of the flat ice sheet in the steep areas along the edge of the Antarctic ice sheet. Additionally, comparing with Fig. 18(b)(c), it indicates that the bias between Sentinel-3 ascending tracks and CryoSat-2 descending tracks is slightly larger than the bias between Sentinel-3 descending tracks and CryoSat-2 descending tracks, that's because Fig. 18(b) contains not only the bias between the two missions but also the AD bias, while Fig. 18(c) contains only the latter. Furthermore, in the study by [51], 23,866 measurement points under CryoSat-2 SARIn mode were collectively analyzed to compare the deviation with Sentinel-3 data. The result showed a deviation of $0.53 \pm 19.1\,\mathrm{m}$, confirming that the bias between these two datasets fluctuates significantly with changes in terrain. This validates the rationality of the results obtained in this study.

B. Dynamic non-linear least squares model

Given the abundant and densely distributed nature of ICESat-2 ATL06 data, this study employs dynamically selected fitting models based on the data density, spatial distribution, and temporal distribution within the gridded segments along the tracks. In contrast to the fixed-plane model used for ICESat data and the fixed-surface model used for CryoSat-2 and Sentinel-3 data, the dynamic fitting models not only improve data utilization efficiency effectively but also provide a more accurate representation of the actual topography, enhancing the precision of extracting elevation changes. Furthermore, for ICESat-2 ATL06 data, this study incorporated a non-linear elevation change term, namely, the elevation change component matrix D. In comparison to the traditional linear temporal variation used in repeated-track fitting models, which assumes a linear change in elevation over time, the surface elevation changes are often non-linear and can be quite complex. In some regions with non-linear trends in ice sheet elevation changes, using linear segments may result in distortion. By replacing linear change terms with non-linear ones, the study effectively avoids distortions in the derived elevation changes, thus improving the accuracy of capturing the dynamics of ice sheet surface elevation changes.

Fig. S9 illustrates the distribution of standard deviations for the three subglacial lakes, with the largest standard deviation around 0.3. In Fig. S10, the error of parameter h_{19} is presented, with the maximum error being around 0.01. It can be observed that the errors do not exhibit a clear spatial pattern. The fitting results show good performance in both gently sloping and steep terrain regions. As a result, this method is applicable to a wide range of terrains.

C. The changes in the outline of the Totten$_2$ subglacial lake

In this paper, we utilized results derived from ICESat-2 ATL06 data to plot the elevation change time series for the three subglacial lakes relative to June 2019 (see Fig. 19), aiming to assess the lake boundaries generated by Smith. Based on the elevation change sequences from 2019 to 2022, it is observed that the derived elevation anomalies for the Totten$_2$ subglacial lake using ICESat-2 exhibit a noticeable mismatch with Smith defined lake boundary. The lake boundary has transformed from its original regular elliptical shape into an irregular form, and there is an overall southeastward shift. This indicates two aspects: firstly, subglacial lake boundaries are not static or stable and can undergo significant shifts through filling-draining cycles. Secondly, the higher spatial resolution data provided by the ICESat-2 satellite can supplement and update sparse, low-precision data from earlier missions to yield critical subglacial lake boundary information, revealing the true dynamic changes in lake boundaries. In the future, it is advisable to integrate the existing lake outlines with the height anomalies derived from ICESat-2 data. Reevaluate the list of active subglacial lakes using ICESat-2 data to refine or update the previous lake outlines. This will enhance the quantification of the dynamic impact of lake activities on the surface ice elevation. Our study has utilized ICESat-2 data to demonstrate that lakes can undergo movement over extended periods, emphasizing the suitability of investigating long-term subglacial lake dynamics based on this phenomenon.

D. Comparison of results for different missions with overlapping times

The study selected three grid cells located within the interiors of the three subglacial lakes, the coordinates of point 1, 2 and 3 are (2076500, -655500), (1965500, -749500), and (2224500, -674500). The time series for the period 2019-2023 was jointly generated using CryoSat-2 and Sentinel-3 data, and the results were compared with the time series generated from ICESat-2 ATL06 data. As depicted in Fig. S11, the two time series exhibit overall consistency in the surface ice elevation changes of the three lakes from 2019 to 2023. However, specific values show some discrepancies, with deviations of approximately 0.1 ± 0.05 meters at the locations of these subglacial lakes. Previous research suggests that there might be factors contributing to the discrepancies between the two time series. Firstly, a typical characteristic of radar altimeters is their ability to penetrate through the overlying snow layer on the ice sheet, causing penetration effects. These effects can vary over time, and despite we have added the backscatter coefficient to the fitting model to reduce the effect of this feature of the radar altimeter on results, it only represents a partial correction and may not completely offset the effects. In addition, there are differences in snow penetration effects between different satellites, resulting

in some of the inter-mission bias. Although we applied the same backscatter coefficient to the radar data from different sources, the remaining effect due to differences in penetration depth of different satellite altimetry measurements should be covered by the inter-mission bias parameters (CS_aCS_d, SEN_aCS_d, SEN_dCS_d). For data from laser altimetry satellites (ICESat and ICESat-2), the snow penetration effect is negligible and therefore the backscatter coefficient is no longer included in the corresponding fitted models [2]. In addition, studies indicate that in regions with complex ice sheet surface topography, the differences between time series generated from CryoSat-2 and ICESat-2 data are more pronounced. The roughness of the ice surface may also introduce biases in the results of radar signal sampling. Additionally, due to the larger footprint of radar altimeters compared to lidar altimeters, the grid size used in fitting radar data needs to be adjusted for optimal fitting results, which is not an issue for lidar data. While these factors are crucial, formal quantification is challenging. For areas with complex terrain at the margins of ice sheets, radar altimetry data may not perform as well as lidar altimetry data in studying real ice surface elevation changes.

E. Subglacial lake hydrological analysis

Hydrological connectivity refers to the existence of connecting channels between subglacial lakes. When the water level in some subglacial lakes continues to rise sufficiently to overcome hydraulic barriers or when effective siphoning is produced through water infiltration from the watershed, lake drainage occurs. Water flows through connecting channels into surrounding subglacial lakes, resulting in the phenomenon of water exchange [1]. The inflow and outflow of subglacial lake water are mainly influenced by the upstream and downstream tributaries. The water from the upstream tributaries, after converging into the main stream, affects the water volume in downstream tributary lakes. Therefore, Totten$_1$ is hydrologically linked to Wilkes$_1$, while changes in the water volume of Totten$_2$ subglacial lake aren't affected by the other two subglacial lakes. During the period from 2003 to 2009, Totten$_1$ experienced relatively frequent inflow and outflow. When the water from the lake converged into the main stream, it flowed downstream, causing an increase in water volume in the downstream Wilkes$_1$ subglacial lake, but the increase was smaller than the decrease in the water volume of upstream Totten$_1$. Between 2010 and 2023, water volume changes in the upstream Totten$_1$ subglacial lake exhibited a slow filling phase followed by a faster filling phase, with no drainage events occurring. Meanwhile, the downstream Wilkes$_1$ subglacial lake remained in a stable state during this period. This indicates that the downstream Wilkes$_1$ subglacial lake responded to the filling events of the upstream Totten$_1$.

Smith categorized hydrological connections between subglacial lakes based on the water volume flowing from one subglacial lake to a nearby lake [39]. The three types of hydrological connections identified are: direct hydrological connection, partial hydrological connection, and no apparent hydrological connection. We conducted a comparative analysis based on previous research, Wright et al. (2012) studied the hydrological linkage between the watershed of the Aurora Subglacial Basin (ASB) in East Antarctica and the ice sheet margin. They concluded that Totten$_2$ subglacial lake, located in the upstream region of the ASB, contributes to the subglacial water flow toward the Totten Glacier, ultimately draining into the ocean beneath the floating ice shelf east of Law Dome [65]. Therefore, the activity of Totten$_2$ subglacial lake was influenced by hydrological changes originating from the upstream ASB region, hundreds of kilometers away. Due to the relatively small selected study area in this paper and the use of different bed topography data, the drainage paths generated in this study differ slightly from those presented by A. P. Wright, but Totten$_2$ was still on a different mainstem than Totten$_1$ and Wilkes$_1$ in their study. Therefore, we hypothesize that Totten$_2$ is not significantly hydrologically connected to Totten$_1$ and Wilkes$_1$.

VI. Conclusions

In this paper, the surface elevation of three subglacial lakes (Totten$_1$, Totten$_2$, and Wilkes$_1$) in the Totten region of Antarctica are analyzed from 2003 to 2023 using a combination of two types of satellite altimeters, ICESat and ICESat-2 (laser altimeters) and CryoSat-2 and Sentinel-3 (radar altimeters), the focus is on studying their hydrological activities. Considering the different data volumes and spatial-temporal distributions, different least squares fitting models are employed for the various datasets. The classic repeat-track algorithm is used for ICESat data, a least squares surface fitting algorithm incorporating the deviation between different missions is used for CryoSat-2 and Sentinel-3, and a dynamic nonlinear least squares fitting algorithm is used for ICESat-2 data. This approach establishes continuous time series of elevation changes for the three subglacial lakes in the Totten region from 2003 to 2023. Additionally, this study combined REMA and BedMachine data to simulate the subglacial drainage pathways in the region, analyzing the hydrological connections among the three subglacial lakes. The long-term elevation change sequences constructed in this study reveal that Totten$_1$ and Totten$_2$ subglacial lakes show overall frequent activity with potential periodicity from 2003 to 2023. Wilkes$_1$ subglacial lake experiences continuous water level increase from 2003 to 2009, followed by a stable state until 2023. The water level changes and subglacial drainage pathways suggest a certain degree of correlation among these three subglacial lakes. The monitoring results of CryoSat-2 and Sentinel-3 with overlapping time intervals are consistent with the results from ICESat-2, demonstrating the capability of ICESat-2 to monitor the activity of active subglacial lakes on shorter time scales. The study also indicates that CryoSat-2 and Sentinel-3 altimeters can serve as a bridge between ICESat and ICESat-2, enabling the monitoring of long-term hydrological activities of active subglacial lakes in Antarctica.

In addition, this study's methods and data have limitations. Firstly, due to differences in satellite configurations and the influence of factors such as snow accumulation and ice surface roughness, the methods used in this study cannot completely eliminate the deviation between different missions. Secondly, limitations in the precision of ice surface elevation and bedrock elevation data may result in discrepancies between the drainage pathways generated in this study and those in previous research. Therefore, further research is needed to rigorously and accurately address the deviation between different missions and to

refine the understanding of the hydrological connections among the three subglacial lakes.

ACKNOWLEDGMENT

The authors would like to thank the European Space Agency for providing CryoSat-2 data and Sentinel-3 data, NASA for providing ICESat data, ICESat-2 data and BedMachine data, PGC for providing REMA.

REFERENCES

[1] S. J. Livingstone *et al.*, "Subglacial lakes and their changing role in a warming climate," *Nat Rev Earth Environ*, vol. 3, no. 2, pp. 106–124, 2022, doi: 10.1038/s43017-021-00246-9.

[2] L. Schröder, M. Horwath, R. Dietrich, V. Helm, and S. R. M. Ligtenberg, "Four decades of Antarctic surface elevation changes from multi-mission satellite altimetry," *The Cryosphere*, vol. 13, no. 2, pp. 427-449, 2019, doi: 10.5194/tc-13-427-2019.

[3] S. Li, J. Liao, and L. Zhang, "Extraction and analysis of elevation changes in Antarctic ice sheet from CryoSat-2 and Sentinel-3 radar altimeters," *J. Appl. Rem. Sens.*, vol. 16, no. 03, p. 034514, 2022, doi: 10.1117/1.JRS.16.034514.

[4] M. R. Siegfried and H. A. Fricker, "Thirteen years of subglacial lake activity in Antarctica from multi-mission satellite altimetry," *Ann. Glaciol.*, vol. 59, no. 76pt1, pp. 42–55, 2018, doi: 10.1017/aog.2017.36.

[5] H. A. Fricker, S. P. Carter, R. E. Bell, and T. Scambos, "Active lakes of Recovery Ice Stream, East Antarctica: a bed rock-controlled subglacial hydrological system," *J. Glaciol.*, vol. 60, no. 223, pp. 1015–1030, 2014, doi: 10.3189/2014JoG14J063.

[6] M. J. Siegert, "Antarctic subglacial lakes," *Earth-Science Reviews*, vol. 50, no. 1, pp. 29–50, 2000, https://doi.org/10.1016/S0012-8252(99)00068-9.

[7] B. Zhang *et al.*, "Elevation Changes of the Antarctic Ice Sheet from Joint Envisat and CryoSat-2 Radar Altimetry," *Remote Sensing*, vol. 12, no. 22, p. 3746, 2020, doi: 10.3390/rs12223746.

[8] A. P. Kapitsa, J. K. Ridley, G. de Q. Robin, M. J. Siegert, and I. A. Zotikov, "A large deep freshwater lake beneath the ice of central East Antarctica," *Nature*, vol. 381, no. 6584, pp. 684–686, 1996, doi: 10.1038/381684a0.

[9] M. J. Siegert *et al.*, "Physical, chemical and biological processes in Lake Vostok and other Antarctic subglacial lakes," *Nature*, vol. 414, no. 6864, pp. 603–609, 2001, doi: 10.1038/414603a.

[10] M. J. Siegert, S. Carter, I. Tabacco, S. Popov, and D. D. Blankenship, "A revised inventory of Antarctic subglacial lakes," *Antartic science*, vol. 17, no. 3, pp. 453–460, 2005, doi: 10.1017/S0954102005002889.

[11] H. A. Fricker, T. Scambos, R. Bindschadler, and L. Padman, "An Active Subglacial Water System in West Antarctica Mapped from Space," *Science*, vol. 315, no. 5818, pp. 1544–1548, 2007, doi: 10.1126/science.1136897.

[12] L. Gray, "Evidence for subglacial water transport in the West Antarctic Ice Sheet through three-dimensional satellite radar interferometry," *Geophys. Res. Lett.*, vol. 32, no. 3, p. L03501, 2005, doi: 10.1029/2004GL021387.

[13] D. J. Wingham, M. J. Siegert, A. Shepherd, and A. S. Muir, "Rapid discharge connects Antarctic subglacial lakes," *Nature*, vol. 440, no. 7087, pp. 1033–1036, 2006, doi: 10.1038/nature04660.

[14] S. P. Carter *et al.*, "Modeling 5 years of subglacial lake activity in the MacAyeal Ice Stream (Antarctica) catchment through assimilation of ICESat laser altimetry," *J. Glaciol.*, vol. 57, no. 206, pp. 1098–1112, 2011, doi: 10.3189/002214311798843421.

[15] S. P. Carter, H. A. Fricker, and M. R. Siegfried, "Evidence of rapid subglacial water piracy under Whillans Ice Stream, West Antarctica," *J. Glaciol.*, vol. 59, no. 218, pp. 1147–1162, 2013, doi: 10.3189/2013JoG13J085.

[16] H. A. Fricker, T. Scambos, S. Carter, C. Davis, T. Haran, and I. Joughin, "Synthesizing multiple remote-sensing techniques for subglacial hydrologic mapping: application to a lake system beneath MacAyeal Ice Stream, West Antarctica," *J. Glaciol.*, vol. 56, no. 196, pp. 187–199, 2010, doi: 10.3189/002214310791968557.

[17] H. A. Fricker and T. Scambos, "Connected subglacial lake activity on lower Mercer and Whillans Ice Streams, West Antarctica, 2003–2008," *J. Glaciol.*, vol. 55, no. 190, pp. 303–315, 2009, doi: 10.3189/002214309788608813.

[18] R. J. Arthern, D. J. Wingham, and A. L. Ridout, "Controls on ERS altimeter measurements over ice sheets: Footprint-scale topography, backscatter fluctuations, and the dependence of microwave penetration depth on satellite orientation," *J. Geophys. Res.*, vol. 106, no. D24, pp. 33471–33484, 2001, doi: 10.1029/2001JD000498.

[19] C. H. Davis, C. A. Kluever, and B. J. Haines, "Elevation Change of the Southern Greenland Ice Sheet," *Science*, vol. 279, no. 5359, pp. 2086–2088, 1998, doi: 10.1126/science.279.5359.2086.

[20] L. S. Sørensen, S. B. Simonsen, R. Meister, R. Forsberg, J. F. Levinsen, and T. Flament, "Envisat-derived elevation changes of the Greenland ice sheet, and a comparison with ICESat results in the accumulation area," *Remote Sensing of Environment*, vol. 160, pp. 56–62, 2015, https://doi.org/10.1016/j.rse.2014.12.022.

[21] H. J. Zwally, R. A. Bindschadler, A. C. Brenner, J. A. Major, and J. G. Marsh, "Growth of Greenland Ice Sheet: Measurement," *Science*, vol. 246, no. 4937, pp. 1587–1589, 1989, doi: 10.1126/science.246.4937.1587.

[22] B. Yang, S. Liang, H. Huang, and X. Li, "An elevation change dataset in Greenland ice sheet from 2003 to 2020 using satellite altimetry data," *Big Earth Data*, pp. 1–18, 2022, doi: 10.1080/20964471.2022.2116796.

[23] B.-H. Kim, C.-K. Lee, K.-W. Seo, W. S. Lee, and T. Scambos, "Active subglacial lakes and channelized water flow beneath the Kamb Ice Stream," *The Cryosphere*, vol. 10, no. 6, pp. 2971–2980, 2016, doi: 10.5194/tc-10-2971-2016.

[24] G. Malczyk, N. Gourmelen, D. Goldberg, J. Wuite, and T. Nagler, "Repeat Subglacial Lake Drainage and Filling Beneath Thwaites Glacier," *Geophys. Res. Lett.*, vol. 47, no. 23, p. e2020GL089658, 2020, doi: 10.1029/2020GL089658.

[25] M. R. Siegfried, H. A. Fricker, S. P. Carter, and S. Tulaczyk, "Episodic ice velocity fluctuations triggered by a subglacial flood in West Antarctica," *Geophys. Res. Lett.*, vol. 43, no. 6, pp. 2640–2648, 2016, doi: 10.1002/2016GL067758.

[26] B. E. Smith, N. Gourmelen, A. Huth, and I. Joughin, "Connected subglacial lake drainage beneath Thwaites Glacier, West Antarctica," *The Cryosphere*, vol. 11, no. 1, pp. 451–467, 2017, doi: 10.5194/tc-11-451-2017.

[27] M. R. Siegfried and H. A. Fricker, "Illuminating Active Subglacial Lake Processes With ICESat-2 Laser Altimetry," *Geophys. Res. Lett.*, vol. 48, no. 14, p. e2020GL091089, 2021, doi: 10.1029/2020GL091089.

[28] Y. Fan *et al.*, "Monitoring the Hydrological Activities of Antarctic Subglacial Lakes Using CryoSat-2 and ICESat-2 Altimetry Data," *Remote Sensing*, vol. 14, no. 4, p. 898, 2022, doi: 10.3390/rs14040898.

[29] M. McMillan, H. Corr, A. Shepherd, A. Ridout, S. Laxon, and R. Cullen, "Three-dimensional mapping by CryoSat-2 of subglacial lake volume changes," *Geophys. Res. Lett.*, vol. 40, no. 16, pp. 4321–4327, 2013, doi: 10.1002/grl.50689.

[30] F. S. Paolo, H. A. Fricker, and L. Padman, "Constructing improved decadal records of Antarctic ice shelf height change from multiple satellite radar altimeters," *Remote Sensing of Environment*, vol. 177, pp. 192–205, 2016, doi: 10.1016/j.rse.2016.01.026.

[31] S. Adusumilli, H. A. Fricker, M. R. Siegfried, L. Padman, F. S. Paolo, and S. R. M. Ligtenberg, "Variable Basal Melt Rates of Antarctic Peninsula Ice Shelves, 1994–2016," *Geophys. Res. Lett.*, vol. 45, no. 9, pp. 4086–4095, 2018, doi: 10.1002/2017GL076652.

[32] L. Sandberg Sørensen, S. B. Simonsen, R. Forsberg, K. Khvorostovsky, R. Meister, and M. E. Engdahl, "25 years of elevation changes of the Greenland Ice Sheet from ERS, Envisat, and CryoSat-2 radar altimetry," *Earth and Planetary Science Letters*, vol. 495, pp. 234–241, 2018, doi: 10.1016/j.epsl.2018.05.015.

[33] Y.-R. Lai and L. Wang, "Monthly Surface Elevation Changes of the Greenland Ice Sheet From ICESat-1, CryoSat-2, and ICESat-2 Altimetry Missions," *IEEE Geosci. Remote Sensing Lett.*, vol. 19, pp. 1–5, 2022, doi: 10.1109/LGRS.2021.3058956.

[34] Qiuyang Zhao, Chunxia Zhou, Qiang Qiang. "Monitoring of subglacial lake activity and hydrological analysis in the East Antarctic Totten Glacier Basin using ICESat altimetry data," *Geomatics and Information Science of Wuhan University*, vol. 42, no. 04, pp. 27-31,2017, doi: 10.14188/j.2095-6045.2017014.

[35] T. Flament and F. Rémy, "Dynamic thinning of Antarctic glaciers from along-track repeat radar altimetry," *J. Glaciol.*, vol. 58, no. 211, pp. 830–840, 2012, doi: 10.3189/2012JoG11J118.

[36] M. A. King, C. S. Watson, and D. White, "GPS Rates of Vertical Bedrock Motion Suggest Late Holocene Ice-Sheet Readvance in a Critical Sector of East Antarctica," *Geophys. Res. Lett.*, vol. 49, no. 4, p. 2021GL097232, 2022, doi: 10.1029/2021GL097232.

[37] A. R. A. Aitken *et al.*, "Repeated large-scale retreat and advance of Totten Glacier indicated by inland bed erosion," *Nature*, vol. 533, pp. 385–389, 2016, https://doi.org/10.1038/nature17447.

[38] E. Rignot and R. H. Thomas, "Mass Balance of Polar Ice Sheets," *Science*, vol. 297, no. 5586, pp. 1502–1506, 2002, doi: 10.1126/science.1073888.

[39] B. E. Smith, H. A. Fricker, I. R. Joughin, and S. Tulaczyk, "An inventory of active subglacial lakes in Antarctica detected by ICESat (2003–2008)," *J. Glaciol.*, vol. 55, no. 192, pp. 573–595, 2009, doi: 10.3189/002214309789470879.

[40] B. E. Schutz, H. J. Zwally, C. A. Shuman, D. Hancock, and J. P. DiMarzio, "Overview of the ICESat Mission," *Geophys. Res. Lett.*, vol. 32, no. 21, p. L21S01, 2005, doi: 10.1029/2005GL024009.

[41] L. Yue, H. Shen, L. Zhang, X. Zheng, F. Zhang, and Q. Yuan, "High-quality seamless DEM generation blending SRTM-1, ASTER GDEM v2 and ICESat/GLAS observations," *ISPRS Journal of Photogrammetry and Remote Sensing*, vol. 123, pp. 20–34, 2017, doi: 10.1016/j.isprsjprs.2016.11.002.

[42] H. J. Zwally *et al.*, "ICESat's laser measurements of polar ice, atmosphere, ocean, and land," *Journal of Geodynamics*, vol. 34, no. 3, pp. 405–445, 2002, https://doi.org/10.1016/S0264-3707(02)00042-X.

[43] Y. Feng *et al.*, "Synthesis of the ICESat/ICESat-2 and CryoSat-2 observations to reconstruct time series of lake level," *International Journal of Digital Earth*, vol. 16, no. 1, pp. 183–209, 2023, doi: 10.1080/17538947.2023.2166134.

[44] M. Meloni *et al.*, "CryoSat Ice Baseline-D validation and evolutions," *The Cryosphere*, vol. 14, no. 6, pp. 1889–1907, 2020, doi: 10.5194/tc-14-1889-2020.

[45] D. J. Wingham *et al.*, "CryoSat: A mission to determine the fluctuations in Earth's land and marine ice fields," *Advances in Space Research*, vol. 37, no. 4, pp. 841–871, 2006, https://doi.org/10.1016/j.asr.2005.07.027.

[46] M. R. Siegfried, H. A. Fricker, M. Roberts, T. A. Scambos, and S. Tulaczyk, "A decade of West Antarctic subglacial lake interactions from combined ICESat and CryoSat-2 altimetry," *Geophys. Res. Lett.*, vol. 41, no. 3, pp. 891–898, 2014, doi: 10.1002/2013GL058616.

[47] D. J. Wingham, L. Phalippou, C. Mavrocordatos, and D. Wallis, "The mean echo and echo cross product from a beamforming interferometric altimeter and their application to elevation measurement," *IEEE Trans. Geosci. Remote Sensing*, vol. 42, no. 10, pp. 2305–2323, 2004, doi: 10.1109/TGRS.2004.834352.

[48] L. Jiang, R. Schneider, O. Andersen, and P. Bauer-Gottwein, "CryoSat-2 Altimetry Applications over Rivers and Lakes," *Water*, vol. 9, no. 3, p. 211, 2017, doi: 10.3390/w9030211.

[49] Q. Yang, Y. Yang, Z. Wang, B. Zhang, and H. Jiang, "Elevation Change Derived from SARAL/ALtiKa Altimetric Mission: Quality Assessment and Performance of the Ka-Band," *Remote Sensing*, vol. 10, no. 4, 2018, doi: 10.3390/rs10040539.

[50] J. Fernández, C. Fernández, E. J. Calero, L. J. Gallardo, H. Peter, and P. Féménias, "The copernicus sentinel-3 missi

on". *ILRS workshop*. pp.1-4, 2016, https://cddis.nasa.gov/lw20/docs/2016/papers/P32-Fernandez_paper.pdf.

[51] J. M. Maddalena, "Elevation and Volumetric changes to the Greenland Ice Sheet derived from Sentinel-3 Satellite Radar Altimetry". University of Bristol, 2022, http://research-information.bristol.ac.uk.

[52] A. Egido and W. H. F. Smith, "Fully Focused SAR Altimetry: Theory and Applications," *IEEE Trans. Geosci. Remote Sensing*, vol. 55, no. 1, pp. 392–406, 2017, doi: 10.1109/TGRS.2016.2607122.

[53] M. McMillan *et al.*, "Sentinel-3 Delay-Doppler altimetry over Antarctica," *The Cryosphere*, vol. 13, no. 2, pp. 709–722, 2019, doi: 10.5194/tc-13-709-2019.

[54] T. Markus *et al.*, "The Ice, Cloud, and land Elevation Satellite-2 (ICESat-2): Science requirements, concept, and implementation," *Remote Sensing of Environment*, vol. 190, pp. 260–273, 2017, https://doi.org/10.1016/j.rse.2016.12.029.

[55] W. Abdalati *et al.*, "The ICESat-2 Laser Altimetry Mission," *Proceedings of the IEEE*, vol. 98, no. 5, pp. 735–751, 2010, doi: 10.1109/JPROC.2009.2034765.

[56] I. M. Howat, C. Porter, B. E. Smith, M.-J. Noh, and P. Morin, "The Reference Elevation Model of Antarctica," *The Cryosphere*, vol. 13, no. 2, pp. 665–674, 2019, doi: 10.5194/tc-13-665-2019.

[57] M. Morlighem *et al.*, "Deep glacial troughs and stabilizing ridges unveiled beneath the margins of the Antarctic ice sheet," *Nat. Geosci.*, vol. 13, no. 2, pp. 132–137, 2020, doi: 10.1038/s41561-019-0510-8.

[58] Jun Liu, Huan Xie, Scaioni Marco, et al. "Analysis of surface height variations in the East Antarctic based on laser altimetry satellite," J*ournal of Tongji University (Natural Science Edition)*, vol. 42, no. 11, pp. 1733-1737+1775, 2014, https://kns.cnki.net/kcms/detail/10.11908/j.issn.0253-374x.2014.11.017.html.

[59] A. A. Borsa, G. Moholdt, H. A. Fricker, and K. M. Brunt, "A range correction for ICESat and its potential impact on ice-sheet mass balance studies," *The Cryosphere*, vol. 8, no. 2, pp. 345–357, 2014, doi: 10.5194/tc-8-345-2014.

[60] B. E. Smith, "Recent elevation changes on the ice streams and ridges of the Ross Embayment from ICESat crossovers," *Geophys. Res. Lett.*, vol. 32, no. 21, p. L21S09, 2005, doi: 10.1029/2005GL024365.

[61] T. Slater *et al.*, "A new digital elevation model of Antarctica derived from CryoSat-2 altimetry," *The Cryosphere*, vol. 12, no. 4, pp. 1551–1562, 2018, doi: 10.5194/tc-12-1551-2018.

[62] M. McMillan, A. Muir, and C. Donlon, "Brief communication: Ice sheet elevation measurements from the Sentinel-3A and Sentinel-3B tandem phase," *The Cryosphere*, vol. 15, no. 7, pp. 3129–3134, Jul. 2021, doi: 10.5194/tc-15-3129-2021.

[63] B. Smith *et al.*, "Ice, Cloud, and Land Elevation Satellite (ICESat-2) Project Algorithm Theoretical Basis Document (ATBD) for Land-Ice Along-Track Products, version 6," 2023, doi: 10.5067/ZQB1BP2DSTGM.

[64] R. L. Shreve, "Movement of Water in Glaciers," *J. Glaciol.*, vol. 11, no. 62, pp. 205–214, 1972, doi: 10.3189/S002214300002219X.

[65] A. P. Wright *et al.*, "Evidence of a hydrological connection between the ice divide and ice sheet margin in the Aurora Subglacial Basin, East Antarctica," *J. Geophys. Res.*, vol. 117, no. F1, p. 2011JF002066, 2012, doi: 10.1029/2011JF002066.

Jun Liu received the B.S. degree in Remote Sensing Science and Technology from Information Engineering University, Zhengzhou, China, in 2006, the M.S. degree in photogrammetry and remote sensing from Southwest Jiaotong University, Chengdu, China, in 2009, and the Ph.D. degree in cartography and geographical information engineering from Tongji University, Shanghai, China, in 2017.

She is currently an Associate Professor at the College of Urban Railway Transportation, Shanghai University of Engineering Science. Her current research interests include satellite laser altimetry and polar remote sensing.

Lihui Chen received the B.S. degree in geomatics engineering from North China University of Water Resources and Electric Power, Zhengzhou, China, in 2022 and she is currently working toward the M.S. degree in Shanghai University of Engineering Science. Her research direction is polar remote sensing.

Denghui Tang received the B.S. degree in railway engineering in 2022 from Shanghai University of Engineering Science, China, where he is currently working toward the M.S. degree. And his research direction is polar remote sensing.

Huan Xie (Senior Member, IEEE) received the B.S. degree in surveying engineering and the M.S. and Ph.D. degrees in cartography and geoinformation from Tongji University, Shanghai, China, in 2003, 2006, and 2009, respectively.

From 2007 to 2008, she was with the Institute of Photogrammetry and GeoInformation, Leibniz Universität Hannover, Hanover, Germany, funded by the China Scholarship Council, as a Visiting Scholar. Her research interests include polar remote sensing and hyperspectral remote sensing.

Xiangbin Cui received his Ph.D. degree in Geological Resources and Geological Engineering from the Department of Earth Sciences at Zhejiang University, China in 2010. After that, he works in Polar Research Institute of China (PRIC) and focuses on studying the Antarctic ice sheet and its potential change through ice sounding radar survey and Radioglaciology. He became a professor in 2021. He has been to Antarctica for six times, and has good experience in geophysical survey design, operation and research in Antarctica.

Peinan Li received the Ph.D.degree in civil engineering from Tongji University, Shanghai, China, in 2014. He is currently an Associate Professor at the College of Environmental Science and Engineering, Donghua University. His current research interests include multi-source data integration and spatio-temporal information prediction.

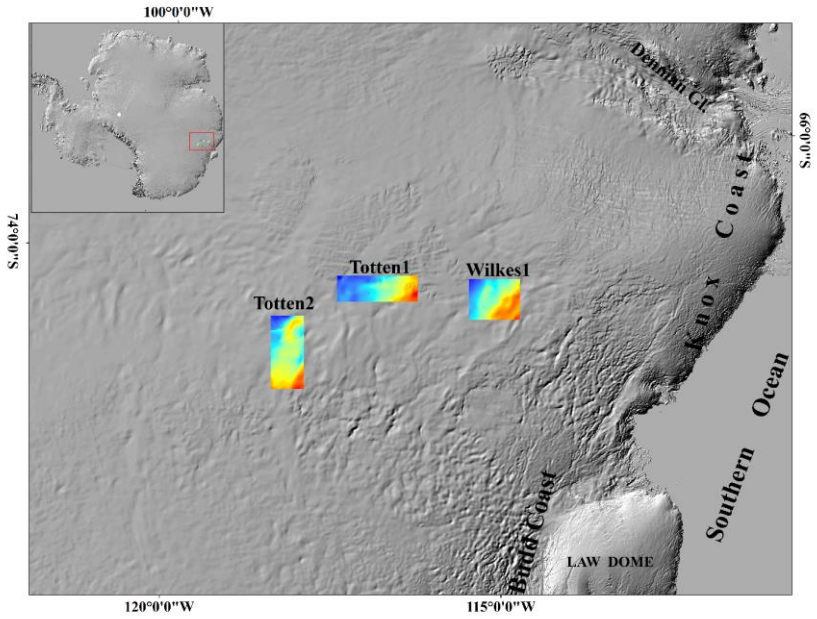

Fig 1. Schematic diagram of the study region

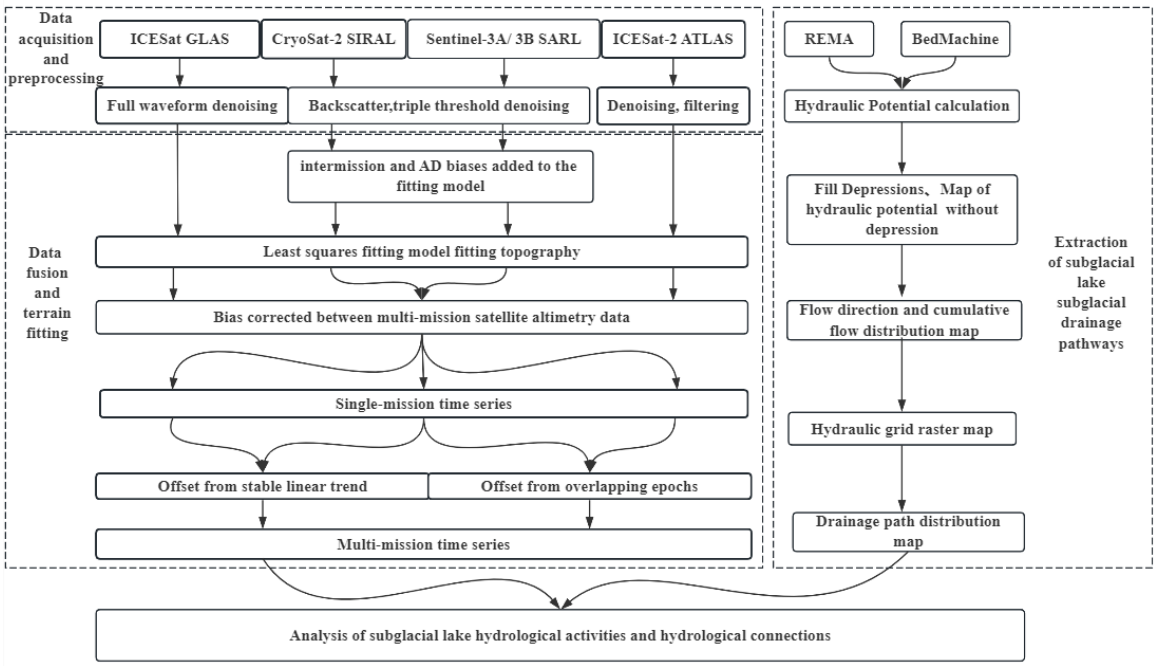

Fig 2. Framework for monitoring the hydrological activities of three subglacial lakes in the Totten Glacier Basin by integrating multi-mission altimetry data.

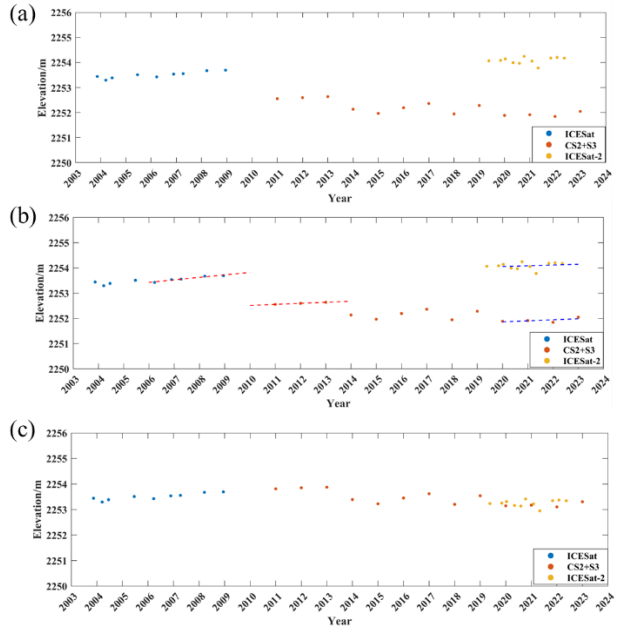

Fig 3. Schematic diagram of intermission biases correction. (a) Single-mission time series of different missions. (b) Off-sets between the different data are determined from trend-corrected elevation differences (red area) or overlapping epochs (blue area) where dh/dt is sufficiently stable. (c) The combined multi-mission time series.

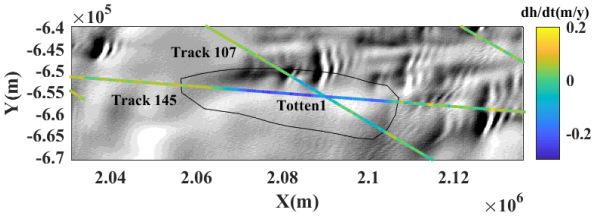

Fig 4. Average elevation change rate of Totten$_1$ from 2003 to 2009 based on ICESat data.

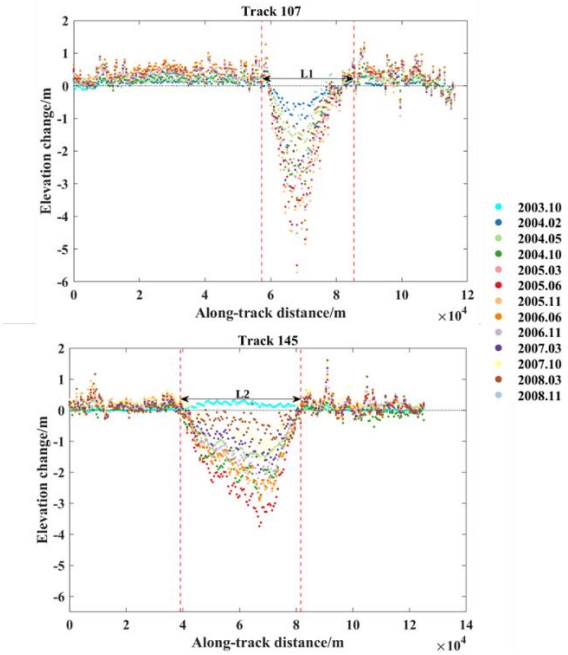

Fig 5. Elevation change of Track 107 and Track 145 from 2003 to 2009.

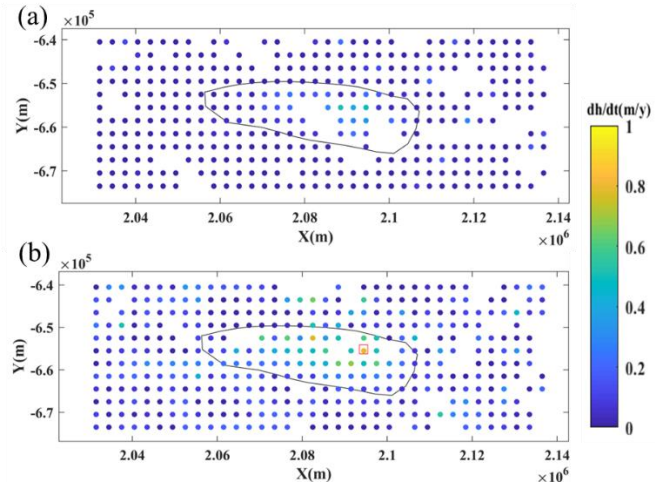

Fig 6. (a) Average surface elevation change rate for Totten$_1$ from 2010 to 2019 based on CryoSat-2 and Sentinel-3 data. (b) Average surface elevation change rate for Totten$_1$ from 2019 to 2023 based on CryoSat-2 and Sentinel-3 data. The red box is the extrema corresponding to the change rate in elevation during this period.

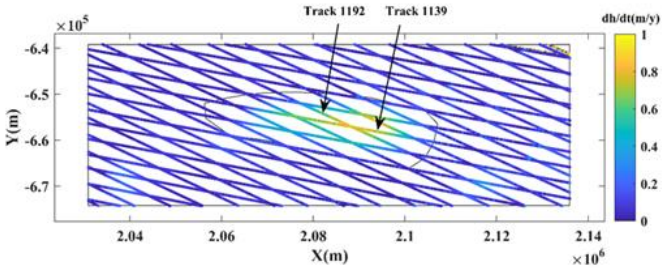

Fig 7. Average surface elevation change rate for Totten$_1$ from 2019 to 2023 based on ICESat-2 data.

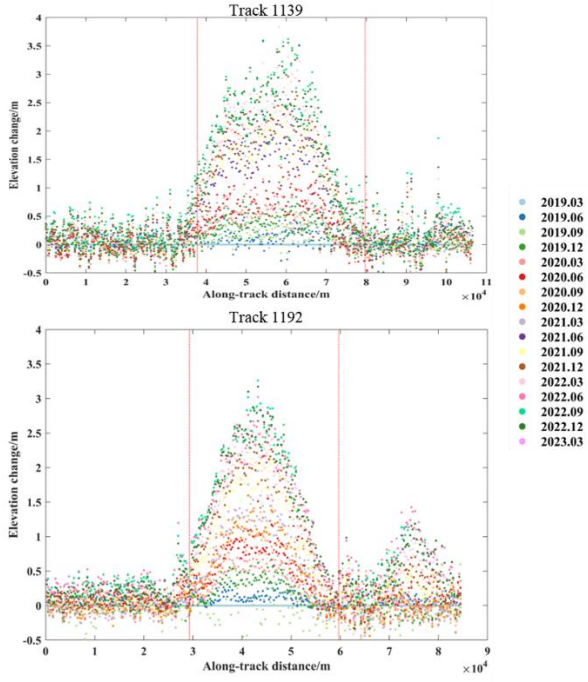

Fig 8. Elevation change results along Track 1139 and Track 1192.

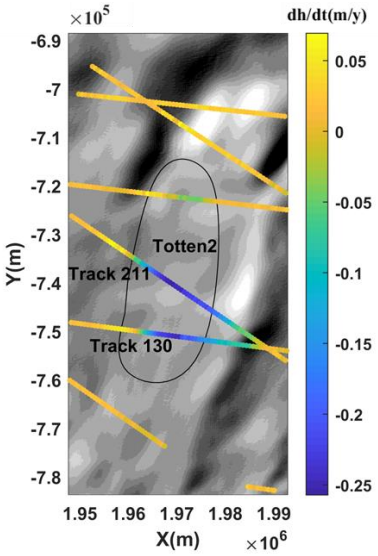

Fig 9. Average elevation change rate of Totten$_2$ from 2003 to 2009 based on ICESat data.

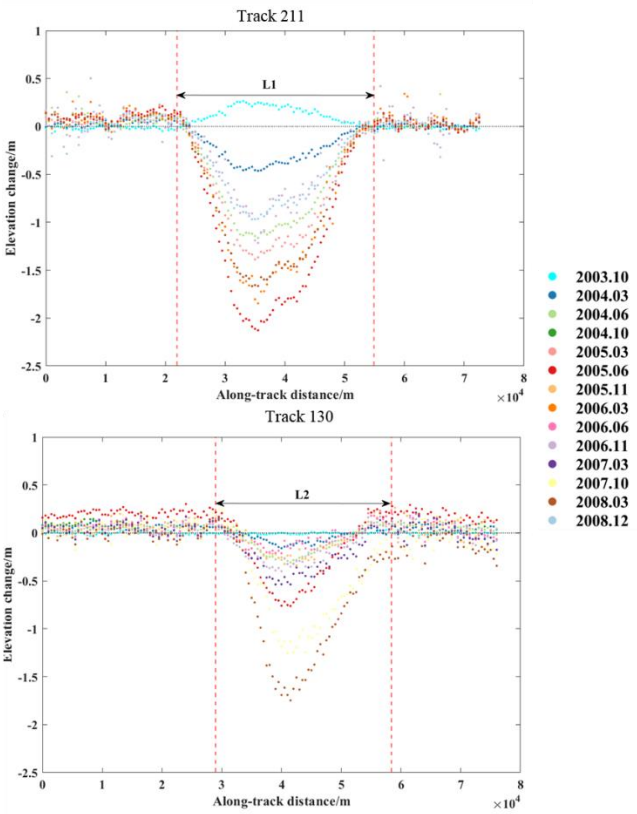

Fig 10. Elevation change of Track 211 and Track 130 from 2003 to 2009.

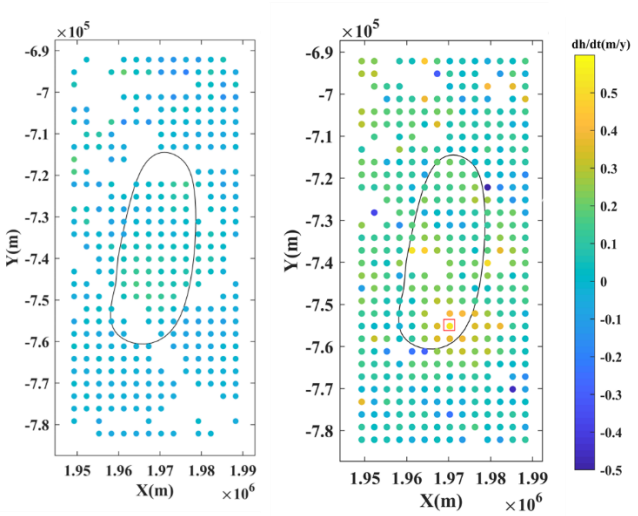

Fig 11. (a) Average surface elevation change rate from 2010 to 2019 based on CryoSat-2 and Sentinel-3 data. (b) Average surface elevation change rate from 2019 to 2023 based on CryoSat-2 and Sentinel-3 data. The red box is the extrema corresponding to the change rate in elevation during this period.

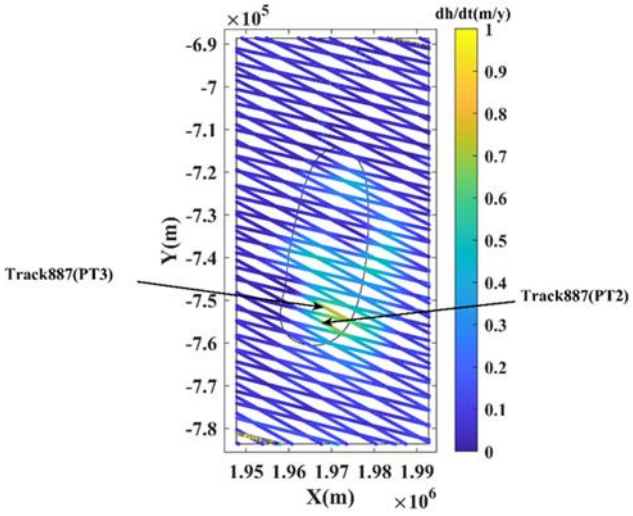

Fig 12. Average surface elevation change rate for Totten$_2$ from 2019 to 2023 from ICESat-2 data.

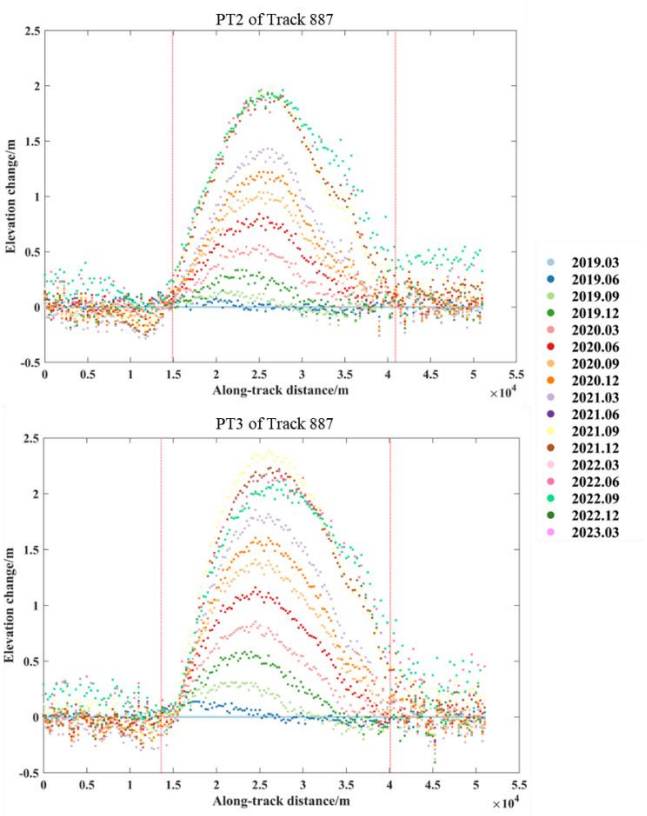

Fig 13. Elevation change results along the two pairs beam of Track 887.

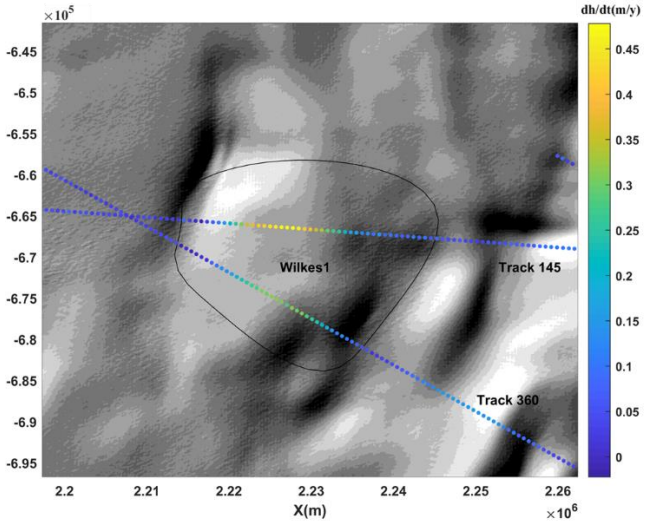

Fig 14. Average elevation change rate of Wilkes$_1$ from 2003 to 2009 based on ICESat data.

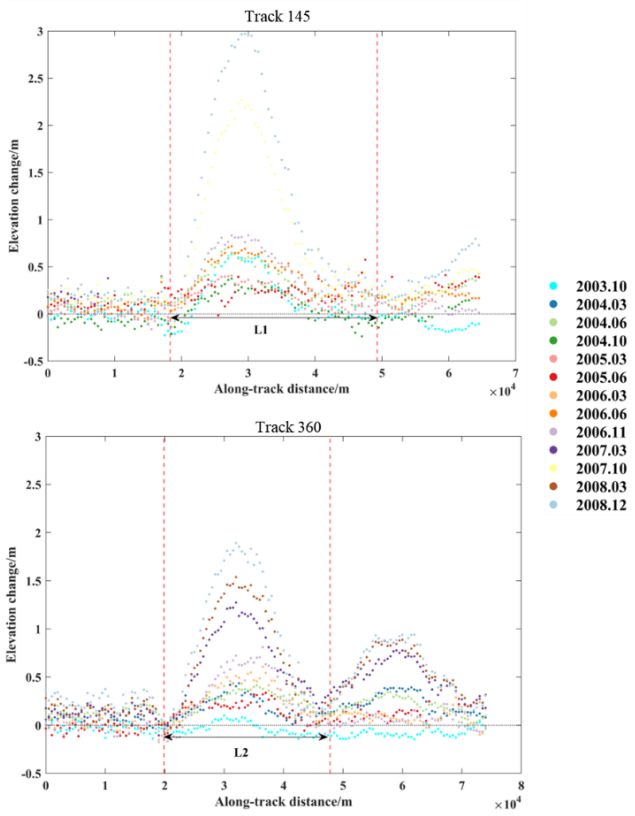

Fig 15. Elevation change of Track 145 and Track 360 from 2003 to 2009.

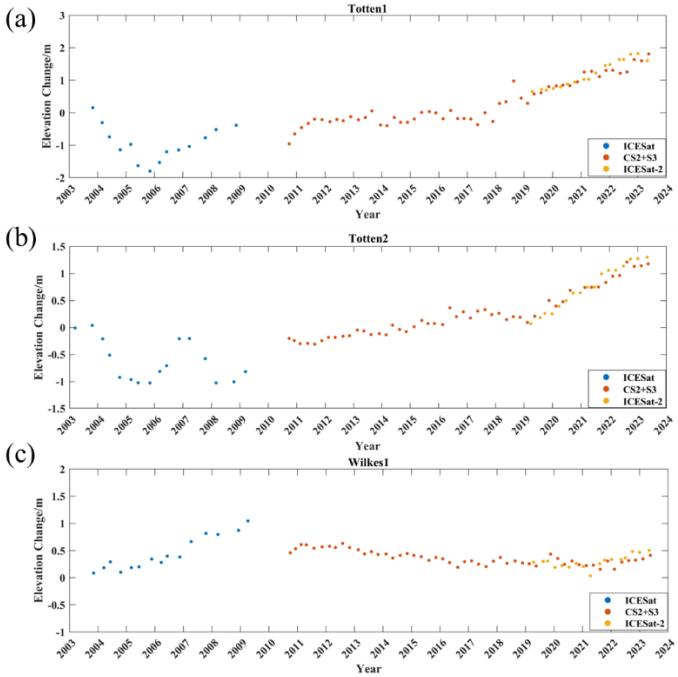

Fig 16. Average elevation change time series of three subglacial lakes from 2003 to 2023.

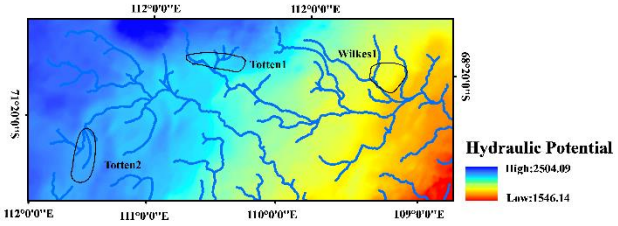

Fig 17. Subglacial Lake Water Flow Path.

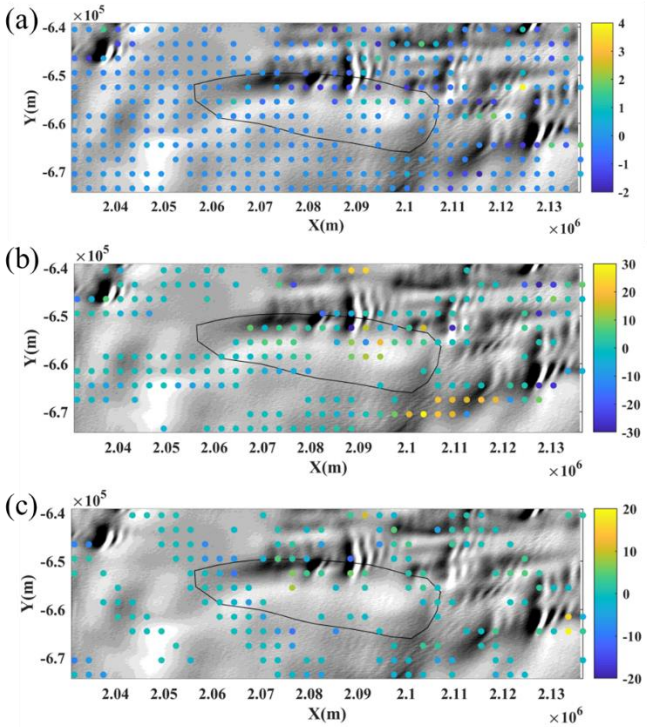

Fig 18. Distribution of three deviation parameter values for CryoSat-2 and Sentinel-3 data. (a) CS_aCS_d. (b) SEN_aCS_d. (c) SEN_dCS_d.

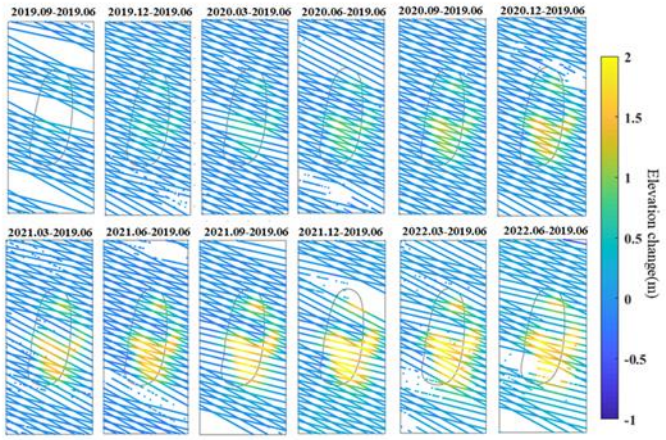

Fig 19. Elevation change time series for $Totten_2$.

TABLE I
COMPARISON WITH PREVIOUS STUDIES

Author	Study time Data	Results $Totten_1$	$Totten_2$	$Wilkes_1$
Qiuyang Zhao	2003-2009 ICESat	-0.117 m/y	periodic changes with a cycle of approximately 33 months, reaching a peak of 1 m	0.18 m/y
Siegfried	2003-2009 ICESat	-0.109 m/y	periodic changes with a cycle of approximately 33 months, reaching a peak of 1.1m	0.1 m/y
	2011-2016 CryoSat-2	0.2 m/y	experienced small height fluctuations	steady state
This study	2003-2009 ICESat	-0.122 m/y	periodic changes with a cycle of approximately 33 months, reaching a peak of 1 m	0.22 m/y
	2010-2019 CryoSat-2 Sentinel-3	0.09 m/y	0.07 m/y	steady state
	2019-2023 CryoSat-2 Sentinel-3 ICESat-2	0.2 m/y	0.2 m/y	steady state

APPENDIX

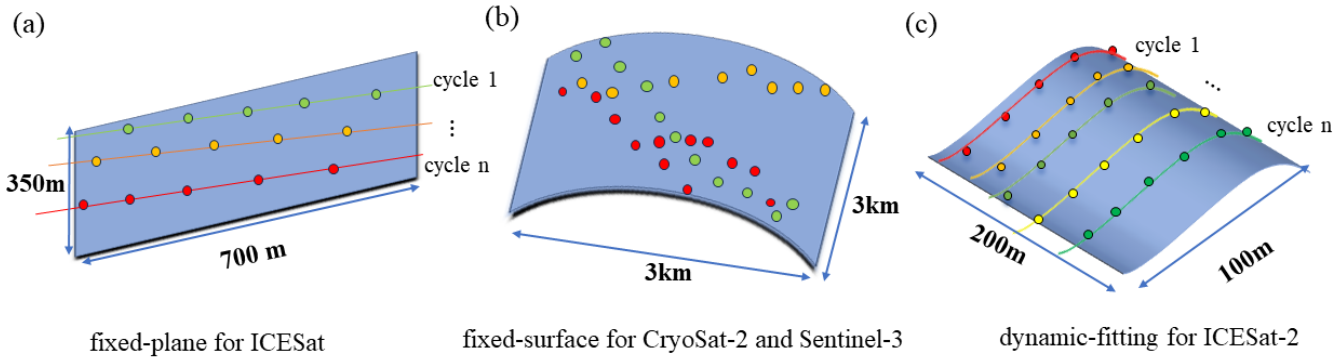

Fig S1. Schematic representation of the three fitting models. For ICESat-2, when the number of data points is less than threshold in the cell, the fitted surface piece is presented as a plane, like (a); when the number of data points in the cell exceeds threshold, the fitted surface is presented as a surface, like (c).

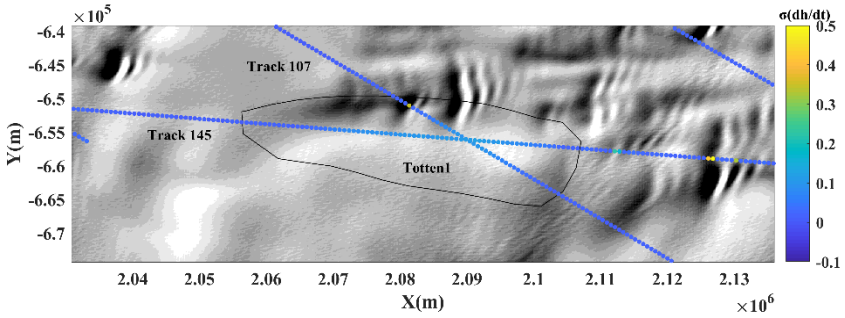

Fig S2. Error of the average elevation change rate of Totten$_1$ from 2003 to 2009.

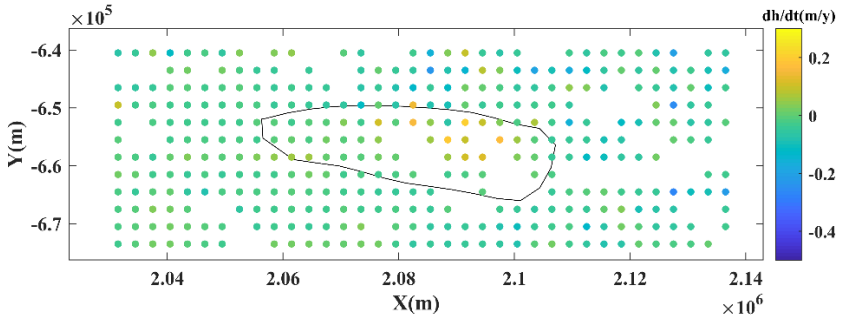

Fig S3. Average surface elevation change rate for Totten$_1$ from 2010 to 2023 from CryoSat-2 and Sentinel-3 data.

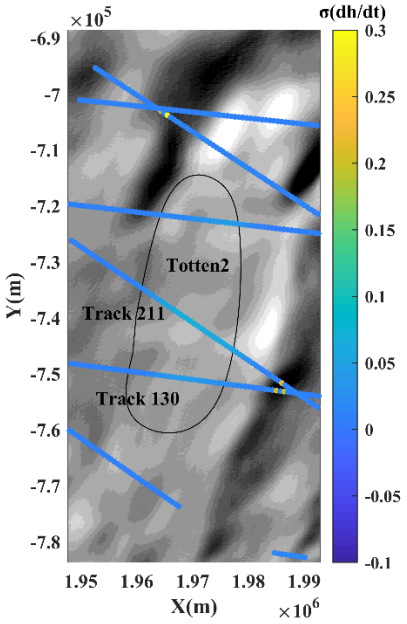

Fig S4. Error of the average elevation change rate of Totten$_2$ from 2003 to 2009.

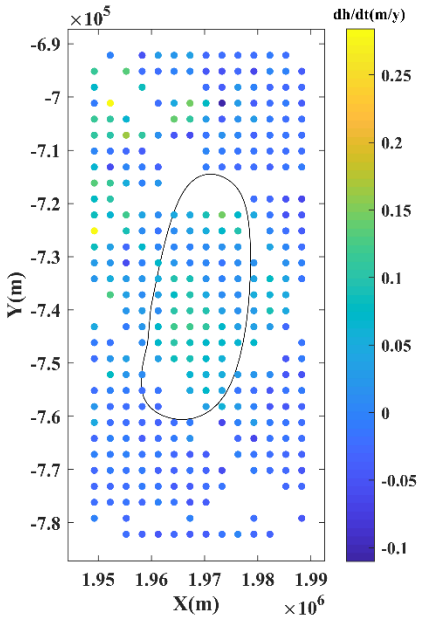

Fig S5. Average surface elevation change rate for Totten$_2$ from 2010 to 2023 from CryoSat-2 and Sentinel-3 data.

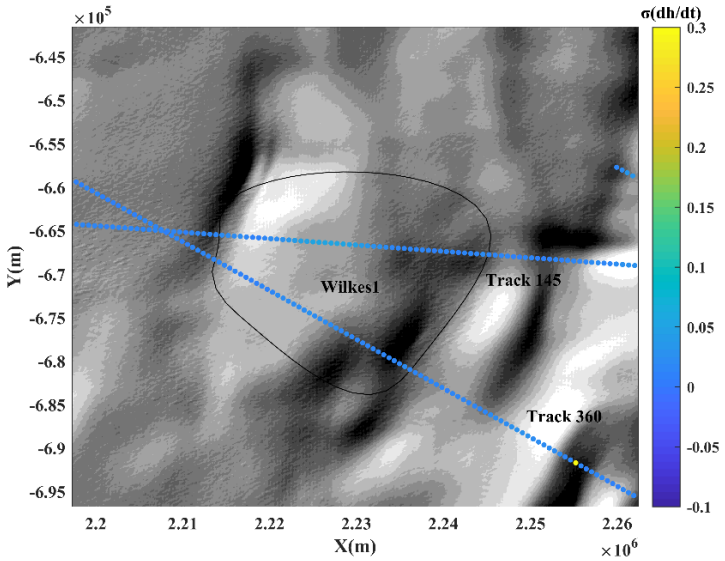

Fig S6. Error of the average elevation change rate of Wilkes$_1$ from 2003 to 2009.

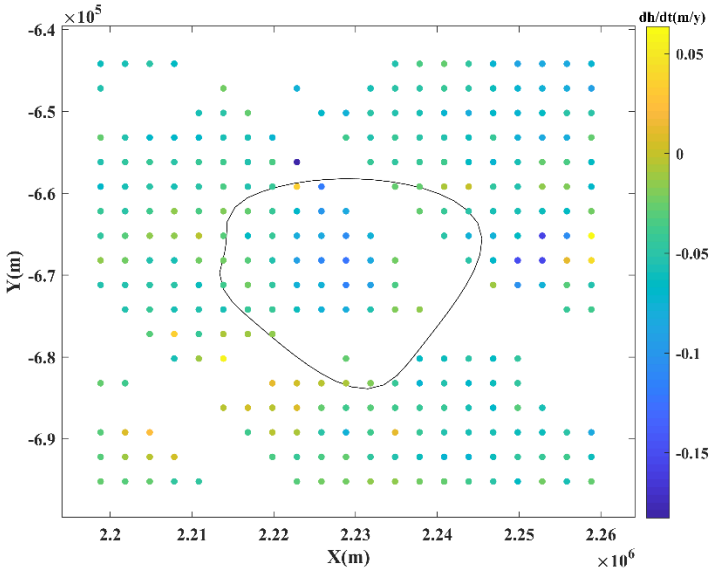

Fig S7. Average surface elevation change rate for Wilkes$_1$ from 2010 to 2023 from CryoSat-2 and Sentinel-3 data.

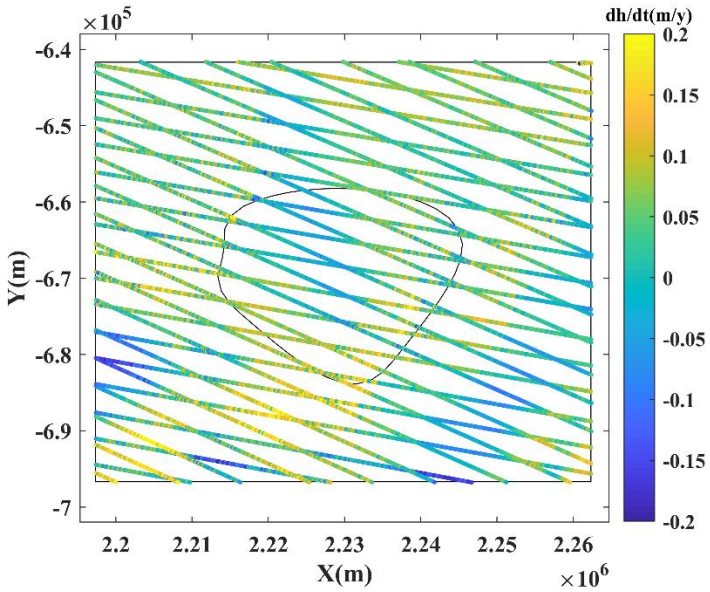

Fig S8. Average surface elevation change rate for Wilkes$_1$ based on ICESat-2 data.

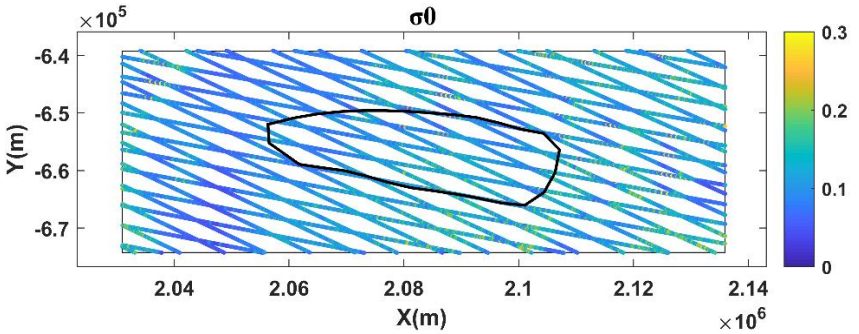

Fig S9. The fitting standard deviation for Totten$_1$ based on ICESat-2.

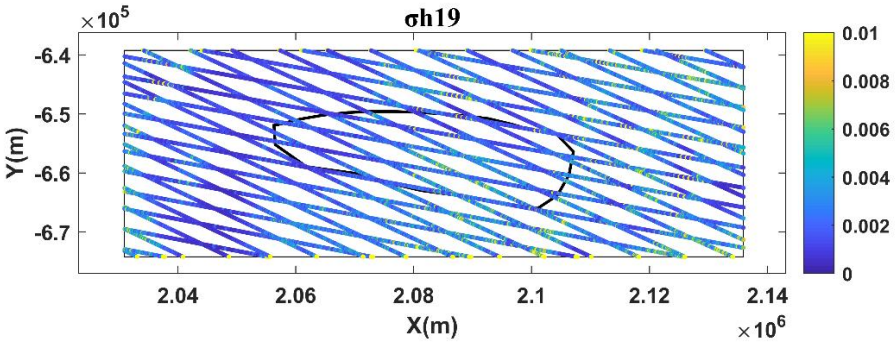

Fig S10. The error of parameter h_{19} forTotten$_1$ based on ICESat-2.

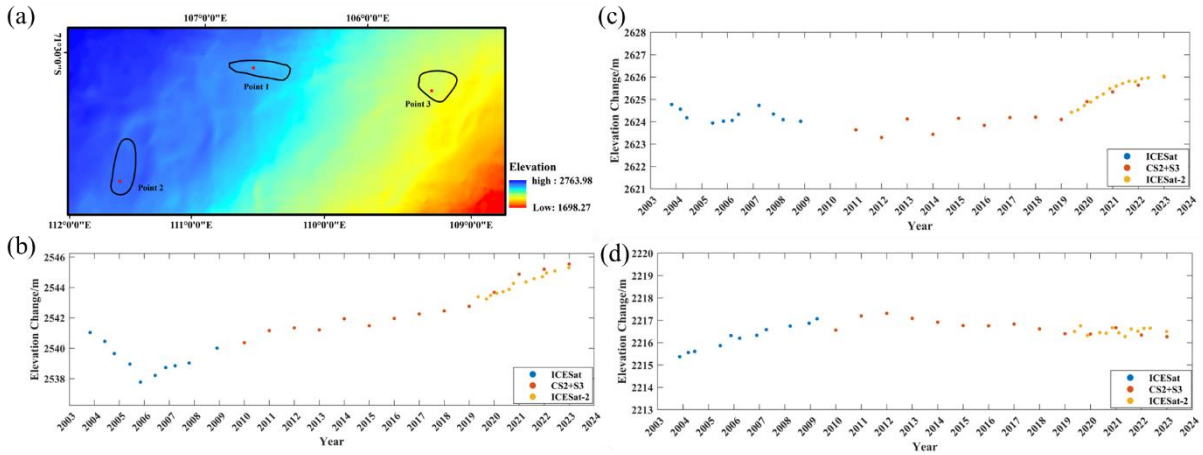

Fig S11. (a) The positions of the selected cells within the interiors of the three lakes; (b) The elevation time series for point 1; (c) The elevation time series for point 2; (d) The elevation time series for point 3.

TABLE SI

SUMMARY OF ALTIMETRY DATA USED IN THE STUDY

Satellite	Years	Cycle	Footprint diameter	Footprint spacing	Website
ICESat	2003.02-2009.10	91 days	~70 m	~170 m	https://nsidc.org/data/icesat
CryoSat-2	2010.08-2023.06	369 days	~1.65 km	~300 m	https://cs2eo.org//
Sentinel-3A	2016.06-2023.06	27 days	300 m	1.6~3 km	https://dataspace.copernicus.eu/
Sentinel-3B	2018.05-2023.06	27 days	300 m	1.6~3 km	https://dataspace.copernicus.eu/
ICESat-2	2018.10-2023.06	91 days	~17 m	~0.7 m	https://doi.org/10.5067/atlas/atl06